Ocean Sci. Discuss., https://doi.org/10.5194/os-2018-62
Manuscript under review for journal Ocean Sci.
Discussion started: 11 June 2018

Ocean Science
Discussions
Open Access
EGU

Tidal variability in the Hong Kong region

Adam T. Devlin

Institute of Space and Earth Information Science, The Chinese University of Hong Kong, Shatin, Hong Kong SAR, China

Jiayi Pan*

Institute of Space and Earth Information Science, The Chinese University of Hong Kong, Shatin, Hong Kong SAR, China

College of Marine Science, Nanjing University of Information Science and Technology, Nanjing, Jiangsu, China

Shenzhen Research Institute, The Chinese University of Hong Kong, Shenzhen, Guangdong, China

Hui Lin

Institute of Space and Earth Information Science, The Chinese University of Hong Kong, Shatin, Hong Kong SAR, China

* - Corresponding author

Ocean Sci. Discuss., https://doi.org/10.5194/os-2018-62
Manuscript under review for journal Ocean Sci.
Discussion started: 11 June 2018

Ocean Science
Discussions
Open Access
EGU

Abstract

Mean sea-level (MSL) is rising worldwide, and correlated changes in ocean tides are also occurring; their combination may influence future total sea-levels (TSL), possibly increasing coastal inundation and nuisance flooding events in sensitive regions. Analyses of a set of tide gauges in Hong Kong and in the South China Sea (SCS) reveal complex tidal behavior. Most prominent in the results are strong correlations of MSL variability to tidal variability which may further increase local flood levels under future MSL rise. We also highlight inter-tidal correlations of diurnal (D_1) tides to semidiurnal (D_2) tides, positively reinforced through the northern SCS, and the correlations of overtide (OT) fluctuations to D_1 and D_2, negatively reinforced (i.e., anti-correlated) across the same region, thought to be related to the baroclinic energetics in the Luzon Strait and the Taiwan Strait. The baroclinic signals may be enhanced at the northern shelf of the SCS and can generate PSI interactions that may amplify minor tides such as M_3. Additionally, there are anomalous tidal events observed in some enclosed harbor regions of Hong Kong, corresponding to times of rapidly changing MSL as well as rapid coastal development projects. Results support the hypothesis that the observed variability is due to multiple spatial processes, best described as an amplification of the local (Hong Kong) tidal response to the prevailing regional (SCS) tidal patterns, enhanced by local harbor changes. A close analysis of the full-spectrum tidal response suggests that a change in the resonant and frictional response may have occurred.

Ocean Sci. Discuss., https://doi.org/10.5194/os-2018-62
Manuscript under review for journal Ocean Sci.
Discussion started: 11 June 2018

1. Introduction

Ocean tides have long been considered to be a stationary process, as they are driven by the gravitational forcing of the Sun and Moon whose motions are complex but highly predictable (Cartwright and Tayler, 1971). Yet, long-term changes in the tides have been observed recently on regional (Ray, 2006; Jay et al., 2009; Zaron and Jay, 2014; Rasheed and Chua, 2014; Feng et al., 2015; Ross et al., 2017) and worldwide spatial scales (Woodworth, 2010; Müller, et al. 2011; Haigh et al., 2014; Mawdsley et al., 2015), concurrent with long-term global mean sea level (MSL) rise (Church and White, 2006; 2011). Since gravitational changes are not the reason, the tidal changes are likely related to terrestrial factors such as: changes in water depth which can alter friction (Arbic et al, 2009), coastal morphology and resonance changes of harbor regions (Cartwright, 1972; Bowen and Gray, 1972; Amin, 1983; Vellinga et al., 2014; Jay et al., 2011; Chernetsky et al., 2010, Familkhalili & Talke, 2016), or stratification changes induced by increased upper-ocean warming (Domingues et al., 2008; Colosi and Munk, 2006; Müller, 2012; Müller et al., 2012), all of which are also related to sea-level rise. Tides can also exhibit short-term variability correlated to short-term fluctuations in MSL. These variabilities may influence extreme water level events, such as storm surge or nuisance flooding (Sweet and Park, 2014; Cherqui et al., 2015; Moftakhari et al., 2015; 2017; Ray and Foster, 2016). Such short-term extreme events are obscured when only considering long-term linear trends. Any significant additional positive correlation between tides and sea-level fluctuations may amplify this effect and implies that flood risk based only on the superposition of present day tides and surge onto a higher baseline sea-level will be inaccurate in many situations. The accurate determination of the nature and impact of sea-level rise and associated tidal change necessitates a regionally- and locally-focused strategy, therefore, analysis of the correlations between tides and sea level can indicate locations where tidal evolution should be considered a substantial modification to sea-level rise. Moreover, since storm surge is a long wave, factors affecting tides can also alter storm surge (Familkhalil and Talke, 2016; Arns et al., 2017), so an improved knowledge of tides can also improve storm response planning and may be instructive in guiding future coastal development.

Recent works have surveyed tidal anomaly correlations (TACs) at multiple locations in the Pacific, examining the sensitivity of tides to sea-level fluctuations (Devlin et al., 2014; Devlin, 2016; Devlin et al., 2017a), finding that over 90% of tide gauges analyzed exhibited some measure of correlation in at least one tidal component. In a related work (Devlin et al.,

Ocean Sci. Discuss., https://doi.org/10.5194/os-2018-62
Manuscript under review for journal Ocean Sci.
Discussion started: 11 June 2018

2017b), the combined TACs of the four largest tidal components was calculated as a proxy for the changes in the highest astronomical tide (δ-HAT), with 35% of gauges surveyed exhibiting a sensitivity of δ-HATs to sea-level fluctuations of at least ±5% in addition to sea-level change. The greatest δ-HAT response was seen in Hong Kong (+65%), and additional analyses revealed that TSL exceedance levels have nearly doubled (+150 mm) that of MSL exceedance alone (+78 mm) over the past 50 years, demonstrating that the non-stationarity of tides can be a significant contributor to total water levels in this region, and this behavior warrants closer examination.

1.1 Sea-level and tides in Hong Kong and the South China Sea

Hong Kong and the Pearl River Delta (PRD) region contains many densely-populated urban metropolises with extensive coastal infrastructure, and substantial recent land reclamation projects. These coastal morphology changes along with sea-level rise may change the local resonant and frictional response of the local tides to the regional tidal variability and may contribute to TSL changes and nuisance flooding. Sea-level rise in the region has exhibited a variable rate in the region over the past 50 years (Li and Mok, 2012), but a common feature of all sea level records in the SCS is a steep increase in the late 1990s with a subsequent decrease in the early 2000s, then followed by a sustained increase to the present day. In addition to the variable MSL behavior, there are also anomalous tidal events observed at gauges in semi-enclosed harbor regions during the late 1990s and early 2000s (shown and discussed below), corresponding to times of both rapidly changing sea level and aggressive land reclamation.

Understanding the tidal behavior in Hong Kong requires a thorough examination of the tidal dynamics in the South China Sea. Both diurnal (D_1) and semidiurnal (D_2) tides enter the SCS from the Pacific through the Luzon Strait. The D_2 constituents are damped by a factor of two as they enter the SCS, and the D_1 constituents are amplified by a similar factor (Zu et al., 2008; Fang et al., 1999; Jan et al., 2007). The semidiurnal wave bifurcates, partially travelling northwest towards the Taiwan Strait, and partially travelling southwest towards the Sunda Shelf, though the diurnal wave only propagates southwest. The part of the semidiurnal wave that travels towards the Taiwan Strait meets the large incoming semidiurnal energy from the East China Sea (ECS). The semidiurnal tides have very large amplitudes (~ 2m) here and exhibit a D_2 resonance on the western side of the Strait via a partial quarter-

Ocean Sci. Discuss., https://doi.org/10.5194/os-2018-62
Manuscript under review for journal Ocean Sci.
Discussion started: 11 June 2018

wave resonance (Jan et al., 2004). In addition, a large amount of D_2 internal energy is generated, though little to no D_1 baroclinic energy is observed.

The Luzon region is one of the most active regions of baroclinic generation in the world ocean (Wang, 2012). Approximately one third of the K_1 surface tide energy (~ 12 GW) is converted to baroclinic energy (Jan et al. 2007), and about one quarter of the M_2 surface tide is converted to the baroclinic tide (Niwa and Hibiya, 2004). The surface tide expression in the SCS is dependent on the baroclinic conversion, which is in turn highly sensitive to the geometric and environmental properties of the Luzon Strait (Jan et al., 2008; Wang, 2012). Internal tides yield a high-mode vertical velocity structure that tends to dissipate tidal energy close to the generation site as well as a low-mode energy that can travel for thousands of kilometers (Liu et al., 2015). Therefore, even at a great distance from the generation site, much of the baroclinic energy may remain coherent. Internal tides can propagate as narrow beams, which may be enhanced upon arrival at the shelf (Lien et al., 2005), and nonlinear interactions are enhanced within the tidal beams, in areas where internal tide beams are reflected (Mercier et al., 2012), or in regions where the tidal beams intersect (Teoh et al., 1997; Korobov and Lamb, 2008).

The D_1 and D_2 internal tides may interact with each other as well as with other frequencies, such as the local inertial frequency, *f*, via parametric subharmonic instability (PSI) interactions (McComas and Bretherton, 1977; MacKinnon and Winters, 2005), a form of resonant triad interactions (Craik, 1985). Previously, such interactions were only thought to occur near the critical latitude (~29° for M_2) where *f* is equal to half the M_2 frequency (see e.g., Alford, 2008). However, for the case where a PSI interaction turns from weakly nonlinear to strongly nonlinear, it can enhance generation at subharmonics different from exactly half the frequency (Korobov and Lamb, 2008). For example, the presence of a resonant triad interaction between M_2 and K_1*O_1 was observed in the Solomon Sea (Devlin et al., 2014). Many PSI-type tidal interactions have been observed in the SCS. Kinetic energy spectra from a current profiler on the northern continental slope near Dongsha Island (~20° N), halfway between the Luzon Strait and Hong Kong) revealed strong peaks at the nonlinear interaction frequencies of fM_1 ($f + M_1$) and M_3 ($M_1 + M_2$), (Xie et al., 2008) as well as other components in the D_3 band (e.g., MO_3). The presence of the PSI interactions was confirmed by bicoherence estimates (Carter and Gregg, 2006), and validates previous suggestions that PSI interactions can occur equatorward of the critical latitudes depending on stratification and

Ocean Sci. Discuss., https://doi.org/10.5194/os-2018-62
Manuscript under review for journal Ocean Sci.
Discussion started: 11 June 2018

circulation conditions (Xie et al, 2011). Other PSI interactions were observed in the southern regions of the SCS (Chinn, 2012; Liu, 2015).

1.2 Outline of this study

It is hypothesized that the observed tidal variability in Hong Kong is due to either: 1) regional changes in the dynamics of the SCS such as MSL rise, circulation patterns, or upper-ocean warming and stratification, 2) local changes in friction and/or resonance related to land reclamation projects, or 3) a combination of coupled mechanisms at multiple spatial and temporal scales. To determine the relevant scales of variability, we perform a spatial and temporal analysis of tidal sensitivity to MSL variations in Hong Kong and the SCS. This manuscript is structured as follows. After the introduction, the data inventory will be described, and a description of the TAC and δ-HAT methods will be given. Following this will be the results, detailing the spatial and temporal patterns of the TAC and δ-HAT determinations. We will then closely examine extreme tidal anomalies in Hong Kong by analyzing the full tidal response, including minor tidal components, and will compare regional correlations of tidal properties in the historical and modern eras. Following the results, a discussion of relevant spatial scales and mechanisms is presented, as well as future proposed works.

2. Methods

2.1 Data sources

A set of 13 tide gauges in the Hong Kong region were provided by the Hong Kong Observatory (HKO) and the Hong Kong Marine Department (HKMD). The longest record is the North Point/Quarry Bay (QB) tide gauge, located in Victoria Harbor. The gauge was established in 1954 and was relocated from North Point to Quarry Bay in 1986, and the datums were adjusted and quality controlled by HKO to provide a continuous record (Ip and Wai, 1990). Five more gauges are provided by HKO: Tsim Bei Tsui (TBT; 1974-present), Tai Po Kau (TPK; 1963-present), Shek Pik (SP; 1999-presnt), Tai Miu Wan (TMW; 1996-present), and Waglan Island (WAG; 1995-present). In addition, four locations are operated by the HKMD (Cheung Chau; CHC, Kwai Chung; KC, Ma Wan; MW, and Ko Lau Wan; KLW); all have been recording from ~2004 to the present day. Next, there are some additional data records originally operated by HKO that are no longer active (Chi Ma Wan (CMW; 1963-1997) and Lok On Pai (LOP; 1981-1999)). Additionally, historical data from China in the Beibu Gulf and the Taiwan Strait are downloaded from the University of Hawaii

Ocean Sci. Discuss., https://doi.org/10.5194/os-2018-62
Manuscript under review for journal Ocean Sci.
Discussion started: 11 June 2018

Sea Level Center (UHSLC; website): Shanwei (SW), Zhapo (ZP), Beihei (BH), Haikou (HK), Dongfang (DF), and Xiamen (XM). These data records are all continuous from 1976-1997, except for Xiamen which runs from 1954-1997. Rounding out this inventory are six other locations in the SCS acquired from UHSLC; Manila (MN) in the Philippines (1984-2016), Kaohsiung (KS) and Keelung (KL) in Taiwan (1980-2014), Vung Tau (VT), Vietnam (1986-2002; 2007-2014); Sedili (SD), Malaysia (1986-2016), Bintulu (BT), Malaysia (1992-2016), and one location on the outside of the SCS closest to the Luzon Strait (Ishigaki Island; IG, 1968-2013) to provide a comparison to the tides within the SCS. The TACs and δ-HATs at these last seven locations were already reported on in Devlin et al. (2017a; 2017b), here, they are recalculated with updated data to compare the spatial coherence of tidal dynamics in the SCS to Hong Kong. Gauge locations in Hong Kong are shown in Figure 1, with the gauges from HKO indicated by green markers, gauges from HKMD by light blue, and historical (non-operational) gauges by red. SCS gauges are shown in Figure 2; green indicates gauges that are actively updated, red indicates gauges that have not been updated since 1997. Table 1 lists the metadata for all locations, including latitude, longitude, and record length.

2.2 Tidal admittance calculations

Investigations of tidal behavior rely on a tidal admittance method. An admittance is the unitless ratio of an observed tidal constituent to the corresponding tidal constituent in the astronomical tide generating force expressed as a potential, V, divided by the acceleration due to gravity, g, to yield $Z_{pot}(t) = V/g$, with units of length that can be compared to tidal elevations, $Z_{obs}(t)$, via harmonic analysis. Yearly harmonic analyses are performed on both $Z_{obs}(t)$ and $Z_{pot}(t)$ at each location, using the R_T_TIDE package for MATLAB (Leffler and Jay, 2009), a robust analysis suite based on T_TIDE (Pawlowicz, 2002). Because nodal and other low-frequency astronomical variabilities are present with similar strengths in both the observed tidal record and in $Z_{pot}(t)$, their effects are eliminated in yearly analyzed admittance time series. The tidal potential is determined based on the methods of Cartwright and Tayler (1971). The result from a single harmonic analysis of $Z_{obs}(t)$ or $Z_{pot}(t)$ determines an amplitude, A, and phase, θ, at the central time of the analysis window for each tidal constituent, with error estimates. A moving analysis window produces time-series of amplitude, $A(t)$, and phase, $\theta(t)$, with the complex amplitude, $\mathbf{Z}(t)$, given by:

$$\mathbf{Z}(t) = A(t)e^{i\theta(t)} . \quad (1)$$

Ocean Sci. Discuss., https://doi.org/10.5194/os-2018-62
Manuscript under review for journal Ocean Sci.
Discussion started: 11 June 2018

The tidal admittance (**A**) and phase lag (**P**) are formed using Eqs. (2) and (3)

$$\mathbf{A}(t) = abs\left|\frac{\mathbf{Z}_{obs}(t)}{\mathbf{Z}_{pot}(t)}\right|, \quad (2)$$

$$\mathbf{P}(t) = \theta_{obs}(t) - \theta_{pot}(t) \quad . \quad (3)$$

The harmonic analysis procedure also provides an MSL time-series. For each resultant dataset (MSL, **A** and **P**), the mean and trend are removed from the time series to allow direct comparison of their co-variability. The magnitude of the long-term trends is typically much less than the magnitude of the short-term variability, which is now more apparent in the data (Devlin et al., 2017a).

Tidal sensitivity to sea-level fluctuations is quantified using tidal anomaly correlations (TACs), the relationships of detrended tidal variability to detrended MSL variability. We determine the sensitivity of the amplitude and phase of individual constituents (M_2, S_2, K_1, O_1, N_2, K_2, P_1, and Q_1) to sea-level perturbations at the yearly-analyzed scale. We also consider the change in the highest astronomical tide (δ-HAT), estimated in two ways. First, by combining the yearly analyzed time series of the four largest tidal amplitudes (M_2, S_2, K_1, and O_1), approximately 75% of the full tidal height (δ-HAT_4), and secondly by considering the combination of all eight constituents, approximately 95% of the full tidal height (δ-HAT_8). The latter determination provides a better approximation to the full tidal range, though the former provides a more statistically stable value, as the four minor constituents are more prone to noise and spurious fluctuations. The detrended time series of the δ-HATs are compared to detrended MSL variability in an identical manner as the TACs, and both are expressed in units of millimeter change in tidal amplitude per 1-meter fluctuation in sea-level. These units are adopted for convenience, though in practice, the observed fluctuations in MSL are on the order of ~ 0.25 m. The phase TACs are reported in units of degree change per 1-meter fluctuation in sea-level.

The TAC methodology can also be used to examine correlations between different parts of the tidal spectrum. We also consider the sensitivity of combined diurnal (D_1; $K_1 + O_1 + P_1 + Q_1$) tidal perturbations to semidiurnal (D_2; $M_2 + S_2 + N_2 + K_2$) tidal perturbations (D_1/D_2 TACs). Additionally, we calculate the sensitivity of tidal range to frictional changes, by considering the combined variations of the seven largest overtides (OT; M_4, M_6, S_4, MK_3, MO_3, SN_4, and MN_4), to fluctuations in the combined D_1 and D_2 amplitude (OT TACs). The units of the D_1/D_2 and OT TACs are dimensionless (i.e., mm/mm), and statistics are

Ocean Sci. Discuss., https://doi.org/10.5194/os-2018-62
Manuscript under review for journal Ocean Sci.
Discussion started: 11 June 2018

calculated as above. We assume that the interannual variability captured by all TACs and δ-HATs can be extrapolated to longer time scales, subject to the qualification that the changes remain "small-amplitude", i.e., a 0.5 to 1m change in MSL and a change in tidal amplitude of a few 10s of cm.

The definition of the year window used for harmonic analysis may have an influence on the value of the TAC or δ-HAT, e.g. calendar year (Jan-Dec) vs. water year (Oct-Sep). To provide a better estimate of the overall correlations for all data we take a set of determinations of the correlations using twelve distinct year definitions (i.e., one-year windows running from Jan-Dec, Feb-Jan, …, Dec-Jan.). We take the average of the set of significant determinations (i.e., *p*-values of < 0.05) as the magnitude of the TAC or δ-HAT. For an estimate of the confidence interval of the TAC or δ-HAT, the interquartile range (middle 50% of the set) is used. A step-by-step description of the TAC and δ-HAT methods, including the details of the calculations of the regressions and statistics can be found in the supplementary materials of Devlin et al. (2017b). For the very long record stations (e.g., QB and TPK), we only consider the past 30 years for TAC and δ-HAT determinations, and for other stations, we use the full record, though some locations are less than 30 years, and some are historical.

We also highlight some anomalous tidal events observed around the turn of the century at certain Hong Kong gauges, and we compare and discuss the coherence and evolution of the tidal behavior in Hong Kong and the SCS via correlation analysis. We consider the eight tides in the D_1 and D_2 band, as well as the $2N_2$, M_3 and MO_3 tides (for reasons that will be made clear later), and MSL. All gauges are compared to the Quarry Bay gauge as the "standard", and we consider a demarcation time between "historical" and "modern" as 1997. For the early record, we use the Hong Kong data at CMW, TPK, LOP, and TBT, the historical data from the mainland of China (to represent the historical SCS). For the modern era, we consider all operational data in Hong Kong, as well as Manila, Vung Tau, Sedili, Ishigaki, and the two Taiwan gauges. We use Ishigaki to represent the Pacific in both time periods. For all comparisons, we only use the data that overlaps the QB record. Due to the nature of the time coverage at our set of gauges, only two gauges will allow a direct comparison in both time periods in Hong Kong (TPK and TBT). However, a few other locations in the historical and modern sub-sets are located close enough to each other to allow a near-direct pairing; Lok On Pai/Ma Wan, and Chi Ma Wan/Cheung Chau.

Ocean Sci. Discuss., https://doi.org/10.5194/os-2018-62
Manuscript under review for journal Ocean Sci.
Discussion started: 11 June 2018

3. Results

The individual TACs for amplitude and phase in Hong Kong and the SCS are discussed first, followed by the δ-HATs, the D_1/D_2 TACs, and the OT TACs. In all figures, significant positive results will be reported by red markers, significant negative results by blue markers, and insignificant values are shown as black markers. The relative size of the markers will indicate the relative magnitude of the TAC or δ-HAT according the legend scale on each plot. All numerical results for the major amplitude TACs (M_2, S_2, K_1, and O_1) are listed in Table 2, and the δ-HATs, D_1/D_2 TACs, and the OT/ (D_1 +D_2) TACs are listed in Table 3. Phase TACs of the major constituents, minor constituent (N_2, K_2, P_1, Q_1) amplitude TACs, and the other OT TACs (i.e., OT/D_1 and OT/D_2) are reported in Table S1, S2 and S3 of the supplementary material. Phase TACs for the minor constituents are insignificant at all locations and are not reported or plotted. Next, we explore the anomalous tidal events seen at Hong Kong gauges in recent years by analyzing the behavior of major and minor tidal components. Finally, we compare correlations between early and later eras to explore the temporal coherency of tidal behavior.

3.1 Tidal anomaly correlations (TACs)

We first show the semidiurnal TACs in Hong Kong (Figure 3 (a) and (c)) and in the SCS (Figure 3 (b) and (d)). In Hong Kong (Fig 3(a)), the strongest positive M_2 TACs are seen at Quarry Bay (+218 ± 37 mm m^{-1}), and at Tai Po Kau (+267 ± 42 mm m^{-1}), with a smaller positive TAC seen at Shek Pik. In the waters west of Victoria Harbor, all gauges except Kwai Chung exhibit moderate negative TACs. In the SCS (Fig 3(b)), very large and positive TACs are seen at the three stations in the Beibu Gulf (Dongfang, Beihei, and Haikou), with values of +190, +460, and +379 mm m^{-1}, respectively. The semidiurnal phase TACs in Hong Kong (shown in the Supplementary materials, Figure S1(a)) show an earlier M_2 tide under higher MSL at QB and TPK (-15 ± 2 and -28 ± 6 deg m^{-1}, respectively), and a later tide west of Victoria Harbor. In the SCS (Fig S1(b)), later tides are observed at Manila, Kaohsiung, and Shanwei, while earlier tides are seen in the Beibu Gulf and at Xiamen. The S_2 results in Hong Kong (Fig 3(c)) reveal that only QB and TPK have significant amplitude TAC values (though smaller than M_2), and the rest of the SCS has a nearly identical spatial distribution as M_2 (Fig 3(d)). The S_2 phase TACs in Hong Kong (Figure S1(c)) again show an earlier tide at QB and TPK under higher MSL, and results in the SCS (Figure S1(d)) are also similar to M_2. The minor semidiurnal amplitude TACs are mainly insignificant in Hong

Ocean Sci. Discuss., https://doi.org/10.5194/os-2018-62
Manuscript under review for journal Ocean Sci.
Discussion started: 11 June 2018

Kong, though N_2 has a significant positive TAC at TPK of +85 ± 12 mm m^{-1} (Figure S2(a)), and K_2 has a small significant TAC at both TPK and QB (Figure S2(c)). In the SCS, all TACs are insignificant or small for N_2 (Figure S2(b)), but the K_2 response in the Beibu Gulf gauges is exceptionally large (+67 to +175 mm m^{-1}), notable for such a small-magnitude constituent (Figure S2(d)).

The diurnal TACs in HK and the SCS generally exhibit a larger-magnitude and more spatially-coherent response than semidiurnal TACs (Figure 4). Like M_2, the strongest K_1 values in Hong Kong (Fig 4(a)) are seen at QB (+220 ± 15 mm m^{-1}) and TPK (+190 ± 68 mm m^{-1}). In the SCS, the largest magnitude TACs are again found in the Beibu Gulf (+180 to +578 mm m^{-1}), but unlike M_2, all significant TACs are positive in the region (Fig 4(b)), and there is a significantly large TAC at Bintulu. The O_1 results in Hong Kong (Fig 4(c)) and in the SCS (Fig 4(d)) are like the M_2 results, showing positive TACs at QB (+146 ± 11 mm m^{-1}) and TPK (+100 ± 25 mm m^{-1}), and strongly negative TACs west of QB. The O_1 response in the SCS is very similar to K_1, though a negative response is now seen at Xiamen and Shanwei, and a small positive response is seen at Keelung. Phase TACs for K_1 are mainly insignificant in Hong Kong (Figure S3(a)), and O_1 phase TACs (Figure S3(c)) are only significant at QB. In the SCS, strong positive phase TACs are seen at Shanwei and Kaohsiung in both K_1 (Figure S3(b)) and O_1 (Figure S3(d)), and negative phase TACs for K_1 and O_1 are seen in the Beibu Gulf. The minor P_1 tide has a positive TAC at QB and Ma Wan (+71 ± 10 and +65 ± 9 mm m^{-1}; Figure S4(a)), and results are coherent throughout the rest of the SCS, with positive responses seen in the Beibu Gulf of + 50 to +153 mm m^{-1}, and all other locations having negative responses of -19 to -55 mm m^{-}(Fig S4(b)). The results for Q_1 are mixed in Hong Kong (Figure S4(c)), with a positive TAC at QB, a negative TAC at Kwai Chung and Chi Ma Wan. The Q_1 TACs are insignificant at all stations in the SCS (Figure S4(d)).

3.2 Change in the highest astronomical tide (δ-HAT)

The TACs are widely observed in Hong Kong and across the SCS. Conversely, the δ-HATs (Figure 5) are only of significance at discrete locations. In Hong Kong, five stations exhibit significant δ-HAT_4 values (Fig 5(a)), with QB and TPK having very large positive magnitudes (+665 ± 85 mm m^{-1} and +612 ± 210 mm m^{-1}, respectively), and Shek Pik having a lesser magnitude of +138 ± 47 mm m^{-1}. Conversely, Ma Wan and Chi Ma Wan exhibit moderate negative δ-HAT_4 values, (~ -100 mm m^{-1}). The same five gauges are significant for

Ocean Sci. Discuss., https://doi.org/10.5194/os-2018-62
Manuscript under review for journal Ocean Sci.
Discussion started: 11 June 2018

347 the δ-HAT_8 determinations (Fig 5(c)), though the overall magnitudes are larger (e.g., +834 ±
348 108 mm m^{-1} at QB and +797 ± 139 mm m^{-1} at TPK). In the SCS, the δ-HAT_4 determinations
349 are extraordinarily large in the Beibu Gulf, with magnitudes of +813 to +1405 mm m^{-1}
350 (Figure 5(b)), and the δ-HAT_8 values are even larger; ~ 20% larger at Haikou and Dongfang,
351 and at Beihei, nearly 60% larger, showing a positive change in tidal range of > 2 meters for a
352 1-meter sea-level fluctuation (Figure 5(d)). Elsewhere in the SCS of note, there are very
353 large δ-HAT values seen at Bintulu, though this is mostly due to the very large D_1 TACs; the
354 D_2 band contributes very little to the change in tidal range here.

355 *3.3 D_1/D_2 TACs and OT TACs*

356 The D_1/D_2 and OT TACs are important in the northern SCS and are less significant in
357 the southern reaches. In Hong Kong, all significant D_1/D_2 TACs results are positive (Figure
358 6(a)), and at most locations the correspondence is nearly 1-to-1 (e.g., QB; +1.08 ± 0.05, TPK;
359 +1.01 ± 0.04, TMW; +1.04 ± 0.20), indicating that a change in D_1 can yield a nearly-identical
360 magnitude change in D_2, and vice-versa. Smaller magnitude relations are seen in the western
361 areas of the domain (e.g., TBT, +0.37 ± 0.02 and LOP; +0.26 ± 0.05). In the SCS (Figure
362 6(b)), the strongest relationships are in the Beibu Gulf. At Beihei, the value is nearly 1-to-1
363 (+1.22 ± 0.03), but at Dongfang, the response is significantly larger than 1 (+2.86 ± 0.19),
364 and at Haikou, the response is less than 1 (+0.61 ± 0.05). Elsewhere, small negative relations
365 are observed near the Taiwan Strait, and large negative relations are seen in the southern
366 SCS.

367 The OT TACs at half of gauges in Hong Kong (Fig 6(c)) and nearly every gauge in
368 the northern SCS (Fig 6(d)) are significant and negatively correlated. Friction is expected to
369 be important in coastal or harbor regions, and indeed, the strongest correlations are found in
370 semi-enclosed or partially protected areas (e.g., QB and Kwai Chung in and near Victoria
371 Harbor, Tsim Bei Tsui in Shenzhen Bay and TPK in Tolo Harbor). The largest OT TAC in
372 Hong Kong is -3.62 ± 0.99 at QB, meaning that for a negative change in the OT component
373 (which would indicate a reduction of friction) of 1 mm, an increase of 3.62 mm will be seen
374 in the forcing tides. In the SCS, the largest (-5.10 ± 0.15) response is seen at Beihei near the
375 end of the Beibu Gulf. The southern parts of the SCS show no significant relations. The OT
376 variability was also compared to the D_1 and D_2 bands individually, shown in the
377 supplementary materials (Figure S5), showing that the D_2/OT relations are generally more
378 coherent.

Ocean Sci. Discuss., https://doi.org/10.5194/os-2018-62
Manuscript under review for journal Ocean Sci.
Discussion started: 11 June 2018

3.4 Anomalous tidal events in Hong Kong

We now examine the temporal behavior of the tides in Hong Kong. In Figure 7, the time series of water level spectrum components are shown for QB and TPK, presenting the D_1 band (a), the D_2 band (b), the OT band (c) and mean sea-level (MSL) (d), given as normalized amplitudes with mean values shown in the legends. Some very notable features of these records are clear. At QB, the early part of the record shows nearly constant tidal amplitudes in D_1, while D_2 amplitudes show a slight decrease, and MSL exhibits a slight positive trend. In the mid-1980s, however, both D_1 and D_2 increase drastically until around the year 2003, at which time both tidal bands undergo a rapid decrease of amplitude of ~15%, sustaining this diminished magnitude for about five years before increasing nearly as rapidly. The OT band shows a sustained increase over the historical record, but many of the fluctuations around the trend are anti-correlated to the perturbations in D_1 and D_2, and during the times of diminished major tides, the OTs increase by about +20%. The MSL record is also highly variable at QB, with a nearly flat trend during the increase in tides seen in the 1980s, followed by a strong increase from ~1993-2000, and then a steep decrease concurrent with the time of diminished tides before increasing again. The gauge at TPK shows a similar tidal behavior, though timings and magnitudes are different here. The increase in D_1 and D_2 at TPK in the 1980s is much larger and peaks earlier than QB, reaching a maximum around 1996, and then decreasing around 1998, about five years before the drop at QB. Both locations experience an absolute minimum around 2007 in D_2, but the D_1 minimum at TPK leads the QB minimum by a few years.

We now examine whether these anomalous events are also apparent at other locations in Hong Kong. In Figure 8, the detrended D_2 variability of all gauges is presented as normalized amplitudes. The longest record gauges (QB and TPK) displayed in Figure 7 are shown as heavy lines (blue and red, respectively), with the other gauges shown as thinner lines according to the legend. Horizontal lines indicate a change of ± 5% from the mean. At QB and TPK, the variability during the anomaly is 10-15% of the mean, but such a large anomaly is not clearly apparent elsewhere, and most other gauges show a variation of only a few percent. There does appears to be a similar pattern suggested at TBT, with an increase from ~1988 to 1995, a decrease until 2007, and an increase afterwards; however, this gauge has some large data gaps during this time, so a confident determination of the tidal behavior is unlikely without more observations. Very similar results are seen when considering the D_1

Ocean Sci. Discuss., https://doi.org/10.5194/os-2018-62
Manuscript under review for journal Ocean Sci.
Discussion started: 11 June 2018

band, shown in the Supplementary material (Figure S6), as well as for the M_2 and K_1 amplitudes (Figures S7 and S8).

3.5 Minor constituent behavior

These anomalies in tidal amplitudes are curious by themselves, however, looking at minor constituents reveals more interesting details. In Figure 9, we present some minor tidal variability as normalized amplitudes for a selection of representative Hong Kong gauges (QB, TPK, TBT, CMW, TMW, MW). The N_2 amplitudes at all Hong Kong stations exhibit a long-period harmonic signal, in phase at all locations, corresponding to the lunar eccentricity cycle of 8.85 years (Fig 9(a)). Typically, this longer-cycle component of the gravitational potential is suppressed in the admittance analyses, but if there is any terrestrial amplification of the N_2 signal, it may be apparent in the post-admittance analyses. There are regular maxima starting from the beginning of the record up to ~2002 at which time a minimum of the cycle is "missed", with the next subsequent minimum being more extreme than all previous minima. This event corresponds with the major anomaly seen in all constituents at QB and TPK. More interestingly, the N_2 signals at Hong Kong tide gauges are all in phase, with a near-simultaneous minimum around 2009. The $2N_2$ tide has a similar gravitational origin as N_2 (Fig 9(b)) and exhibits a similar long-period harmonic signal of ~ 4.425 year (8.85/2 year). Before the anomaly period, the $2N_2$ signal is relatively uncorrelated and noisy, but after ~2000, the spatial coherence of $2N_2$ increases, while the N_2 coherency decreases. After 2009, the harmonic signal is no longer evident in N_2, as there is no clear maximum in ~2013. The M_3 tide, usually small (<5 mm) and noisy in the ocean, is significant at all Hong Kong gauges (~15-25 mm), and also exhibits a ~ 8.85-year signal at all gauges (Fig 9(c)). There is again a large anomaly present at all gauges after the turn of the 21st century, though the M_3 minimum leads the N_2 minimum by a few years due to a phase shift. Another component of the D_3 spectrum, the MO_3 tide, also displays a coherent 8.85-year signal (Fig 9(d)). This tidal constituent is typically thought of as a shallow-water overtide but can also arise via nonlinear interactions between M_2 and O_1.

The spatial coherence of the minor tides is not as clear in the greater SCS. Figure 10 displays the same constituents at selected gauges in the SCS. We use Quarry Bay again (to represent Hong Kong), Xiamen (to represent the Taiwan Strait), Dongfang (to represent the Beibu Gulf), Vung Tau (to represent the central SCS), Sedili (to represent the Gulf of Thailand) and Ishigaki (to represent the Pacific Ocean). The N_2 tide is very strong within the

Ocean Sci. Discuss., https://doi.org/10.5194/os-2018-62
Manuscript under review for journal Ocean Sci.
Discussion started: 11 June 2018

Taiwan Strait (~350 mm at Xiamen), and of moderate amplitude elsewhere (Fig 10(a)). The long-period harmonic signal is also present at most gauges with a similar relative variability, though Dongfang is more variable and noisy, and no other locations shows such a large relative anomaly as QB circa 2009. The $2N_2$ tide is less coherent regionally than Hong Kong (Fig 10(b)), though the correlations between Vung Tau and Sedili do appear to be slightly better after ~2000. At Xiamen, $2N_2$ has the largest observed magnitude (~ 50 mm), and the ~4.425 yr signal is strong, but opposite in phase to QB. For M_3, the long-period signal is generally not observed to be strong in areas of the SCS away from Hong Kong. However, Xiamen does show a large relatively variable signal, which, like $2N_2$, is opposed in phase to QB. Finally, the MO_3 tide (Fig 10(d)) does not appear to be important away from Hong Kong; there is a signal suggested at Ishigaki, but the mean value is very small (~ 3 mm), and this may be attributed to noise.

3.6 Early correlations vs. modern correlations

From looking at Figures 7 through 10, it is apparent that there is more variability in the later years of the record than in the earlier parts of the record. This suggests the possibility of a recent regime change in the tidal behavior in the Hong Kong and SCS and warrants a closer examination. We compare the correlations of QB with other gauges in Hong Kong and the SCS for both the "historical" and "modern" data sets described above to determine the relevant spatial and temporal scales of tidal variability, including the minor constituents considered in Figures 9 and 10. Correlation values for M_2, K_1, M_3, MO_3, N_2, and $2N_2$ amplitudes are given in Table 4. Table S3 gives the correlations for S_2, O_1, K_2, P_1, Q_1, and MSL. Table entries give two entries for longer gauges who cover both time periods (e.g., QB, TPK, and IG), as well as a few station pairs that are close enough geographically to allow a direct comparison (CMW/CHC and LOP/MW), separated by a "/". Gauges that do not have data during either period will be indicated by a "~". Additionally, the average correlation at all gauges in HK and the SCS are given for both eras, and the better correlation between eras will be indicated by bold text.

Results show that the tidal correlations in the region are generally less significant in the later record than the early record. At Tai Po Kau, all constituents have a strong correlation in early years (+0.63 to +0.83) but show a lesser correlation in later years (+0.16 to +0.60). At Tsim Bei Tsui, however, the correlation is somewhat better in later years for semidiurnal constituents. The comparison of Lok On Pai to Ma Wan shows lesser

Ocean Sci. Discuss., https://doi.org/10.5194/os-2018-62
Manuscript under review for journal Ocean Sci.
Discussion started: 11 June 2018

correlations in later years (+0.06 to +0.76) than in early years (+0.35 to +0.87), and the same situation is seen when comparing Cheung Chau (+0.02 to +0.61) to Chi Ma Wan (+0.34 to +0.69). The average correlations of Hong Kong gauges are lower in later years than in early years; e.g. the M_2 average correlation decreases from +0.62 to +0.28, and K_1 from +0.54 to +0.31. In the SCS, historical M_2 and K_1 average correlations are +0.45 and +0.48, but the modern correlations are much smaller (both ~ +0.17). The N_2 tide is highly correlated to QB in both time periods at nearly all gauges in HK and the SCS, due to the long-period harmonic discussed above, but these correlations have decreased from +0.75 in HK and +0.66 in the SCS to +0.67 and +0.48, respectively. The exception to the pattern of decreasing correlations is the $2N_2$ tide, whose correlations increase in the modern era (+0.59 to +0.86 in HK and +0.29 to 0.41 in the SCS). The M_3 tide is highly correlated to QB at most HK gauges (+0.75 to +0.90) which shows similar correlations in both eras; but in the SCS, the M_3 correlations are only strong near HK at Zhapo, Shawei, and Xiamen (though at Xiamen, the tide is anti-correlated to QB). Finally, The MO_3 tide is highly correlated at all locations in HK (+0.78 to +0.92), having increased slightly in the modern era, but in the SCS is only important very near to HK (Zhapo and Shanwei). These correlation changes confirm what was suggested by Figure 9 and 10.

4. Discussion

4.1 Spatial scales of tidal variability

This survey has identified several varieties of tidal variability in Hong Kong and the SCS that suggest multiple spatial scales of importance. The TAC (Figures 3 and 4) and δ-HAT (Figure 5) results appear to be more important on a local basis, as the strongest responses are mainly concentrated at specific locations (e.g., The Beibu Gulf, QB and TPK). These locations also have significant positive correlations of the four largest tidal amplitudes to a positive MSL fluctuation, and both locations show a negative response (earlier arriving tide) of semidiurnal tidal phases. Other locations show a mixed result. The M_2 response is negative at gauges just west of QB (CHC, CMW, MW) and positive at SP, with a similar pattern seen for the O_1 and Q_1 amplitude TACs. Conversely, the K_1 TAC results are generally positive. Minor constituent TACs are generally unimportant in Hong Kong, but TPK is more sensitive to the semidiurnal minor tides, while QB tends to be more sensitive to the diurnal band. At both QB and TPK, the positive reinforcements of individual tidal fluctuations lead to very large δ-HAT_4 and δ-HAT_8 values, though large negative δ-HAT_4 and δ-HAT_8 values

Ocean Sci. Discuss., https://doi.org/10.5194/os-2018-62
Manuscript under review for journal Ocean Sci.
Discussion started: 11 June 2018

507 are seen near to QB at CMW and MW. The spatial connections in the semi-enclosed center
508 harbor regions suggest a connected mechanism; this area is where the majority of recent
509 Hong Kong coastal reclamation projects have occurred, including the construction of a new
510 island for an airport, shipping channel deepening and other coastal morphology changes.
511 Such changes in water depth and coastal geometry strongly suggest a relation to frictional or
512 resonance changes. The TACs in the Beibu Gulf are strongly positive for most constituents,
513 and the δ-HATs are even larger than those seen at Hong Kong. Away from Hong Kong and
514 the northern SCS, TAC and δ-HATs are of less significance.

515 The D_1/D_2 TAC relations (Figures 6 (a) and (b)) are a more regionally-relevant
516 phenomenon, being significant nearly everywhere in Hong Kong and in the northwest and
517 north-central SCS, and less significant in the Taiwan Strait and the southern SCS. The
518 majority of significant D_1/D_2 TACs are positive, with most being nearly 1-to-1 (i.e., a ~1-mm
519 change in D_1 will yield a ~1-mm change in D_2), confirmed by the close similarity of tidal
520 behavior of the D_1 and D_2 tidal bands in Hong Kong (e.g., Figure 7 and Figure 8). This
521 aspect of tidal variability in Hong Kong is likely related to the dynamics near the Luzon
522 Strait, where large amounts of baroclinic conversion in both D_1 and D_2 tides tend to couple
523 the variabilities (Jan et al., 2007; 2008; Lien et al., 2015). The low-mode baroclinic energy
524 can travel great distances, being enhanced upon arrival at the shelf and leading to the further
525 generation of energy at non-traditional frequencies such as *f* and M_3 (Xie et al., 2008; 2011;
526 2013).

527 There are two sub-regional exceptions to the D_1/D_2 correlations. First, the western
528 part of Hong Kong the relationships are markedly less than 1 to 1 (~0.33 to ~0.25 at TBT and
529 LOP, respectively). This may be partially influenced by effects of the Pearl River, which
530 discharges part of its flow along the Lantau Channel. The flow of the river is highly seasonal
531 and ejects a freshwater plume at every ebb tide that varies by prevailing wind conditions and
532 by the spring-neap cycle (Gu et al., 2012; Pan et al, 2014). The plumes may affect turbulence
533 and mixing in the region and can dissipate energy away the tidal bands, which may
534 "decouple" the correlated response of D_1 and D_2. This may also help explain the insignificant
535 value seen at Zhapo just to the west of Hong Kong within the influence of the river. The
536 second sub-region is in the Taiwan Strait. Here, there is a larger amount of semidiurnal
537 baroclinic energy than diurnal, as part of the D_2 wave that enters through the Luzon Strait
538 travels north through the Taiwan Strait to meet the incoming D_2 wave from the East China
539 Sea, leading to a pronounced resonance along the Taiwan coast (though not along the coast of

Ocean Sci. Discuss., https://doi.org/10.5194/os-2018-62
Manuscript under review for journal Ocean Sci.
Discussion started: 11 June 2018

China, due to the irregular topography of the cross-section. (Jan et al., 2004). However, there is no significant diurnal wave or internal tide in the Taiwan Strait, so the semidiurnal constituents dominate here, and is thus decoupled from the diurnal variability.

The OT TAC results in Hong Kong and the SCS show a generally negative relation (Figure 6 (c) and (d)). The sensitivity of shallow-water overtides (OT) to fluctuations in the forcing tides are most significant at harbor locations and along the southeastern reaches of Hong Kong. In the SCS, OT TACs are most important in the Beibu Gulf and near the Taiwan Strait, further suggesting the importance of friction in these dynamic regions. The strength of forcing tides and shallow-water overtides should both be dependent on the depth and morphology, so such a inverse relationship is to be expected in general. However, the implications of the frictional response can be complex under scenarios of rising sea levels (e.g., Hollemann and Stacey, 2014). For a sea-level rise along a shore with a gently sloping bottom, such as a beach, rising sea levels will inundate more low-lying areas, increasing friction and dissipating energy from the forcing tides. By contrast, harbors are deeper and flat-walled, often deepened further to develop navigation channels or accommodate shipping terminals. For these regions, sea-level rise will decrease friction, as the distance from the bottom will increase without new land areas being inundated, hence, less energy will be dissipated from the forcing tides. This in turn may have indirect effects on the total sea levels in other regions near the deep harbor areas. In either situation, the relations of OTs to forcing tides will be negative. Interestingly, the OT TACs are insignificant in the southern SCS; since these regions are the shallowest in the study domain, they should be subject to large frictional tides, yet they are not correlated to the forcing tides as they are in the northern SCS. This may be at least partly attributable to the dominant importance of seasonal processes in the Gulf of Thailand reported on by Devlin et al. (2018) and may be indicative of the OT TAC relations in the northern SCS being more closely related to baroclinic activity than water depth, since baroclinic energy is less important in very shallow regions.

4.2 Effects of regional tidal variability on local variability

The presence of strong M_3 and MO_3 tides at most gauges in Hong Kong (Fig 9) indicates a connection to the dynamics at the shelf where significant D_3 energy has been observed (Xie et al., 2008). The N_2 tide with its typical ~8.85 yr periodicity is largest in the Taiwan Strait, but closer to Luzon and elsewhere in the SCS, N_2 is much smaller. This suggests that the source of the long-period signal in M_3 and MO_3 is the N_2 energy originating

572 in the Taiwan Strait. The N_2 wave may couple with the incoming D_1 and D_2 energy from
573 Luzon at the northern SCS shelf and may intensify PSI and triad interactions. The M_3 and
574 MO_3 signals are likely initially generated near the shelf, and then may be enhanced by N_2
575 energy from the Taiwan Strait which imparts the long-period modulation to the D_3 band,
576 leading to coherent D_3 signals with long-period modulations observable in Hong Kong. A
577 resonance in M_3 has been observed before on the shelf near Brazil in the south Atlantic
578 (Huthnance, 1980), demonstrating that a large M_3 can result from a combination of an "organ
579 pipe" quarter wave resonance from the tide that leads to high amplitudes at the shore (Webb,
580 1976), and a half-wave transverse resonance that enhances the tides at the edge of the shelf.
581 Such a mechanism is also possible near Hong Kong, which is at a similar latitude as Brazil,
582 and the shelf in the SCS near Hong Kong has similar depth, width, and slope characteristics
583 as the Brazil shelf. This hypothesis is further supported by noticing that the long-period
584 modulation is strongest in the Taiwan Strait and northern shelf region but diminishes further
585 away (Fig 10). In the Beibu Gulf and the southern SCS, the N_2 variation is almost
586 nonexistent, and the M_3 signal is much smaller. Outside the SCS in the Pacific (Ishigaki), the
587 M_3 tide is virtually nonexistent, with no significant periodicity seen.

588 The usually insignificant $2N_2$ tide is also interesting, being more spatially coherent
589 than N_2 in Hong Kong after ~2000, before the anomalous event (Fig 9(b)). This suggests that
590 the anomaly could be related to a resonance shift due to the combination of rising sea-levels
591 and the anthropogenically modified coastal morphology. Since the N_2 and $2N_2$ frequencies
592 are close (within 2%), is it possible that the extensive changes to the coastal morphology have
593 shifted the dominant resonance by a similar amount, yielding the anomaly event as a
594 harmonic adjustment to new forcing conditions. It may alternatively be related to a regional
595 change in the SCS (e.g., rising MSL or increased stratification due to upper-ocean warming).
596 However, since data coverage is sparse in the SCS, and few locations allow direct
597 comparisons of "before and after", any conclusions based on this limited data would be hasty.
598 Local and regional models may help to determine which spatial scale is most relevant.

599 Hong Kong has had a long history of land reclamation to accommodate an ever-
600 growing infrastructure and population, including the building of a new airport island (Chep
601 Lap Kok), land connections and from the Kowloon Peninsula to Stonecutters' Island and
602 channel deepening to accommodate container terminals, and many bridges, tunnels, and "new
603 cities", built on reclaimed land (e.g., Tai Po and Tseung Kwan O). All of these may have
604 changed the resonance and/or frictional properties of the region. Tai Po Kau has also seen

some land reclamation efforts, such as Science Park, that have changed the coastal morphology. Both locations also show coherent D_1/D_2 and OT TACs, as well as having the largest δ-HATs, and the largest tidal anomalies in the 2000s. Other locations in Hong Kong did not show such extreme variations, so these variations appear to be amplified in harbor areas. Decreases in friction associated with sea-level rise in the SCS may lead to higher forcing tides, and those changes may also be amplified by the close correlations of D_1 and D_2 variability or local harbor development which may further decrease local friction. Hence, a small change in friction due to a small sea-level change may induce a significant change in tidal amplitudes. The positive reinforcement of multiple tides correlated with regional sea-level adjustments may amplify the risks of coastal inundation and coastal flooding, as evidenced by the gauges that had the largest δ-HAT values.

4.3 Limitations of this study and future steps

The inventory of tide gauges provided by HKO and the HKMD has revealed new dynamics and spatial connectivity in the area. However, some gauges are of short length and/or riddled with data gaps, making a full analysis of the area problematic. For example, the Tsim Bei Tsui (TBT) gauge covers a long period, but there are significant gaps in the record, which complicates our analysis. This gauge is located within a harbor region (Deep Bay), bordered to the north by Shenzhen, PRC, which has also grown and developed its coastal infrastructure in past decades, therefore, one might expect similar dynamics are was seen at QB and TPK. While there were significant OT TACs, and D_1/D_2 correlations at TBT, no significant TACs or δ-HATs were observed. The large anomalies seen at QB and TPK around 2000 are suggested by the data at TBT, but some of the missing data corresponds to this time. Without more data or observations, no answers can be concluded about this location at the present time. However, future studies will examine this region via remote sensing and *in-situ* data to better understand the tidal behavior in this area, since the Deep Bay region is highly ecologically sensitive, being populated by extensive mangrove forests which may be disturbed by rapidly changing sea levels (Zhang et al., 2018), so accurate determination of future sea-levels is of utmost importance to the vitality of these important ecosystems.

Furthermore, there is only limited historical data available in the rest of the SCS, most of it having not been updated in 20 years. This complicates efforts to understand the full spatial and temporal extent of the tidal variability in the greater SCS region. A caveat is also

637 made about the very large TACs and δ-HATs observed in the Beibu Gulf; these are likely due
638 to the sensitive resonance in the Gulf, and it is unlikely that such large-magnitude changes
639 will remain linear over such large MSL fluctuations (i.e., it violates the "small-amplitude"
640 assumption taken above). Yet, the behavior in the region is still worthy of future study.
641 Another limitation comes from the nature of the harmonic analysis technique used
642 (R_T_TIDE) which only resolves energy at discrete tidal frequencies. This will not be able
643 to identify tidal energy at the local (latitude-dependent) inertial frequency, f (at Hong Kong,
644 $T_f \sim 31.625$ hr), which may be a significant component of the energy cascade (Xie et al.,
645 2008; 2011;2013; Chinn et al., 2012). It is also likely that the M_1 tide is part of the cascade,
646 yet this tide was below the noise limit at all gauges analyzed here. However, since the M_1
647 interactions are an intermediate step that transfers energy to M_3 (i.e., M_2 to M_1, then to M_3 via
648 $M_2 + M_1$), this energy is high-frequency and not detectable at the yearly-analyzed scale.
649 Finally, there are only surface observations available (i.e., tide gauges), though the tidal
650 velocities are also variable at depth. The installation of current profilers at inland and
651 offshore locations near Hong Kong could provide beneficial observations of the three-
652 dimensional dynamics, could reveal the presence of energy at lesser frequencies such as M_1
653 and f as well as being able to separate the baroclinic component of the tides. Previous current
654 profiler observations in the Hong Kong waters are currently being analyzed, to be presented
655 in a future study. Finally, the tidal variability could be better explored via utilization of
656 analytical and numerical models. This is beyond the scope of the current observational study
657 but is the subject of an ongoing project.

658 ***5. Conclusions***

659 This study has presented new information about the tidal variability in Hong Kong,
660 based on observations of a set of historical and modern tide gauges in Hong Kong and in the
661 South China Sea. The observed dynamics support the hypothesis that the changes are due to
662 multiple processes and are best described as an amplification of the local (Hong Kong) tidal
663 response to changes in the prevailing regional (SCS) tidal patterns, which may have been
664 enhanced by local harbor changes and land reclamation. The D_1/D_2 and OT TACs, on the
665 other hand, are more likely due to the internal tide dynamics near the Luzon Strait which are
666 enhanced at the shelf; this may influence the tidal behavior in other parts of the SCS and may
667 also explain the large spatial scale of these correlations, as well as explaining the presence of
668 M_3. The large TACs and δ-HATs in Hong Kong and the anomalous events in tidal
669 amplitudes seen at the Quarry Bay and Tai Po Kau gauges are likely due to a combination of

changing resonance and friction induced by coastal improvement projects which may amplify the regional D_1/D_2 and OT TACs in harbor regions. These anomalies also suggest that a regime change in tidal resonance has occurred, with the effect being most pronounced at gauges in semi-enclosed harbors where all tidal components are strongly modulated via the conservation of the D_1/D_2 ratios. A shift in the tidal regime is further suggested by the less significant spatial correlations of most tidal components (except $2N_2$) observed in recent years as compared to historical eras.

Overall, the tidal variability seen in Hong Kong may have significant impacts on the future of total sea-levels in the region. Short-term inundation events, such as nuisance flooding, may be amplified under scenarios of higher sea-levels that lead to corresponding changes in the tides, as evidenced by the strong D_1/D_2 and OT connections and very large TACs which may amplify small changes in water levels or reductions in friction due to harbor improvements. It is probable that changes in harbor geometry have influenced tidal evolution in Hong Kong as a cumulative effect of all projects. Future studies will perform simple analytical models as well as high resolution three-dimensional models to simulate changing coastlines under a variety of sea-level, tidal forcing, and anthropogenic change scenarios (historical and future) to better understand the tidal dynamics in Hong Kong at the local scale (e.g., how much morphological change in a harbor region would be needed to shift the dominant resonance from N_2 to $2N_2$), conditions that allow or enhance PSI or resonant triad interactions, and the utilization satellite-derived tidal observations and models in the South China Sea to better understand the dynamics at the regional scale, particularly the D_1/D_2 ratios, and the M_3 prevalence in the SCS.

Code availability All code employed in this study was developed using MATLAB, version R2011B. All code and methods can be provided upon request.

Data Availability The data used in this study from the Hong Kong Observatory (HKO; www.hko.gov.hk) and the Hong Kong Marine Department (HKMD; www.mardep.gov.hk/en/home.html) was provided upon request, discussion of intentions of use, and permission from the appropriate agency supervisors. Data used from the University of Hawaii Sea Level Center (UHSLC; www.uhslc.soest.hawaii.edu) is publicly available.

Author Contributions ATD did all analyses, figures, tables, the majority of writing, and complied the manuscript. JP provided editing, insight, guidance, and direction to this study. HL provided critical and helpful input.

Competing Interests The authors declare they have no competing interest.

Acknowledgements This work is supported by The National Basic Research Program of China (2015CB954103), the National Natural Science Foundation of China (project 41376035), the General Research Fund of Hong Kong Research Grants Council (RGC) (CUHK 402912 and 403113), the Hong Kong Innovation and Technology Fund under the grants (ITS/259/12 and ITS/321/13), and the direct grants of the Chinese University of Hong Kong.

730 **FIGURE CAPTIONS:**

731 **Figure 1** Tide gauge locations in Hong Kong used in this study. Green markers indicate
732 active gauges provided by the Hong Kong Observatory (HKO), light blue markers indicate
733 gauges provided by the Hong Kong Marine Department (HKMD), and red markers indicate
734 historical gauges once maintained by HKO that are no longer operational.

735 **Figure 2** Tide gauge locations in the South China Sea (SCS). All tide gauge data is provided
736 by the University of Hawaii Sea Level Center; green markers indicate actively recording and
737 updated tide gauges, and red markers indicate historical gauges that have not been publicly
738 updated since 1997.

739 **Figure 3** Semidiurnal tidal anomaly correlations (TACs) of detrended M_2 amplitude to
740 detrended MSL in (a) Hong Kong, (b) the South China Sea, and of detrended S_2 amplitude to
741 detrended MSL in (c) Hong Kong, and (d) the South China Sea. Red markers indicate
742 positive TACs and blue indicates negative TACs, with the marker size showing the relative
743 magnitude according to the legend. Black marks indicate insignificant TACs. Map
744 backgrounds in (b) and (d) show mean tidal amplitudes over the period of 1993-2014 (color
745 scale, meters) and phases (solid lines, 30° increment), taken from the ocean tidal model of
746 TPXO7.2, (Egbert and Erofeeva, 2002, 2010).

747 **Figure 4** Diurnal tidal anomaly correlations (TACs) of detrended K_1 amplitude to detrended
748 MSL in (a) Hong Kong, (b) the South China Sea, and of detrended O_1 amplitude to detrended
749 MSL in (c) Hong Kong, and (d) the South China Sea. Red markers indicate positive TACs
750 and blue indicates negative TACs, with the marker size showing the relative magnitude
751 according to the legend. Black marks indicate insignificant TACs. Map backgrounds in (b)
752 and (d) show mean tidal amplitudes over the period of 1993-2014 (color scale, meters) and
753 phases (solid lines, 30° increment), taken from the ocean tidal model of TPXO7.2, (Egbert
754 and Erofeeva, 2002, 2010).

755 **Figure 5** Results of the δ-HAT_4 determinations, the correlation of detrended ($M_2 + S_2 + K_1 +$
756 O_1) to detrended MSL in Hong Kong (a) and the SCS (b), and results of the δ-HAT_8
757 determinations, the correlation of detrended ($M_2 + S_2 + N_2 + K_2 + K_1 + O_1 + P_1 + Q_1$) to
758 detrended MSL in Hong Kong (c) and the SCS (d). Red markers indicate positive TACs and
759 blue indicates negative TACs, with the marker size showing the relative magnitude according
760 to the legend. Black marks indicate insignificant TACs.

761 **Figure 6** Results of the D_1/D_2 TACs, the correlation of detrended D_2 ($M_2 + S_2 + N_2 + K_2$) to
762 detrended D_1 ($K_1 + O_1 + P_1 + Q_1$) in Hong Kong (a) and the SCS (b), and results of the OT
763 TACs, the correlation of detrended ($D_1 + D_2$) to detrended OT($M_4 + M_6 + MK_3 + MO_3 + MS_4$
764 $+ MN_4 + S_4$) in Hong Kong (c) and the SCS (d). Red markers indicate positive TACs and
765 blue indicates negative TACs, with the marker size showing the relative magnitude according
766 to the legend. Black marks indicate insignificant TACs.

767 **Figure 7** Time series of water level spectrum components at the Quarry Bay (QB; blue) and
768 Tai Po Kau (TPK; red) tide gauges in Hong Kong, showing the D_1 band (a), the D_2 band (b),
769 the OT band (c) and mean sea-level (MSL) (d). Components are plotted as a function of
770 normalized amplitudes to show relative variability, with mean values given in the legend.

Ocean Sci. Discuss., https://doi.org/10.5194/os-2018-62
Manuscript under review for journal Ocean Sci.
Discussion started: 11 June 2018

771 **Figure 8** Time-series of the detrended D_2 water level spectrum component at all tide gauges
772 in Hong Kong, plotted as a normalized amplitude to show relative variability, with mean
773 values given in the legend. Each gauge is indicated by color according to the legend, with the
774 QB (solid blue) and TPK (solid red) gauges shown as heavier lines. Horizontal dotted lines
775 indicate the ±5% variational band relative to the mean amplitude.

776 **Figure 9** Minor constituent variability at selected Hong Kong gauges. N_2 is shown in (a),
777 $2N_2$ in (b), M_3 in (c) and MO_3 in (d). All quantities are plotted as normalized amplitudes to
778 show relative variability, with mean values given in the legends at the right.

779 **Figure 10** Minor constituent variability at selected South China Sea gauges. N_2 is shown in
780 (a), $2N_2$ in (b), M_3 in (c) and MO_3 in (d). All quantities are plotted as normalized amplitudes
781 to show relative variability, with mean values given in the legends at the right.

782
783
784
785
786
787
788
789
790
791
792
793
794
795
796
797
798
799
800
801
802
803

Ocean Sci. Discuss., https://doi.org/10.5194/os-2018-62
Manuscript under review for journal Ocean Sci.
Discussion started: 11 June 2018

804 **FIGURES**

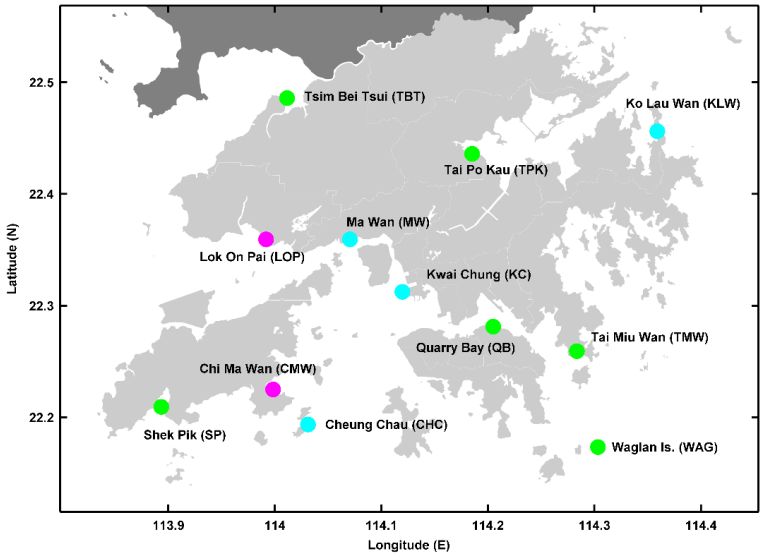

805

806 **Figure 1** Tide gauge locations in Hong Kong used in this study. Green markers indicate
807 active gauges provided by the Hong Kong Observatory (HKO), light blue markers indicate
808 gauges provided by the Hong Kong Marine Department (HKMD), and red markers indicate
809 historical gauges once maintained by HKO that are no longer operational.

810

811

812

813

814

815

816

817

818

819

820

821

822

Ocean Sci. Discuss., https://doi.org/10.5194/os-2018-62
Manuscript under review for journal Ocean Sci.
Discussion started: 11 June 2018

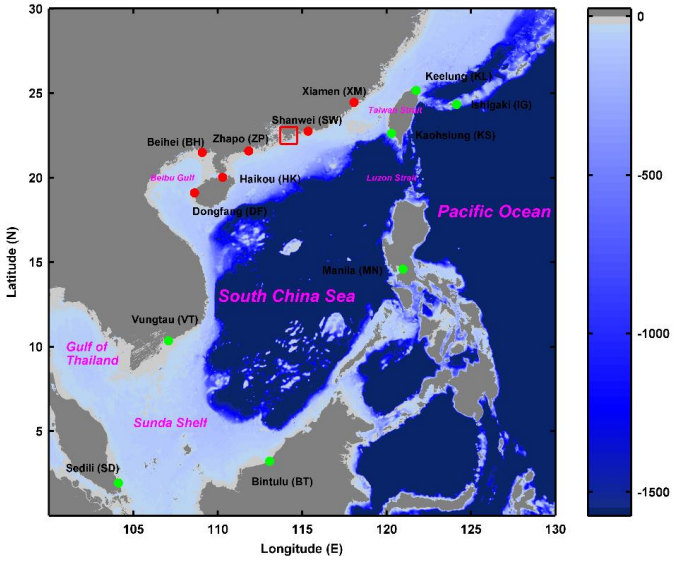

Figure 2 Tide gauge locations in the South China Sea (SCS). All tide gauge data is provided by the University of Hawaii Sea Level Center; green markers indicate actively recording and updated tide gauges, and red markers indicate historical gauges that have not been publicly updated since 1997.

Ocean Sci. Discuss., https://doi.org/10.5194/os-2018-62
Manuscript under review for journal Ocean Sci.
Discussion started: 11 June 2018

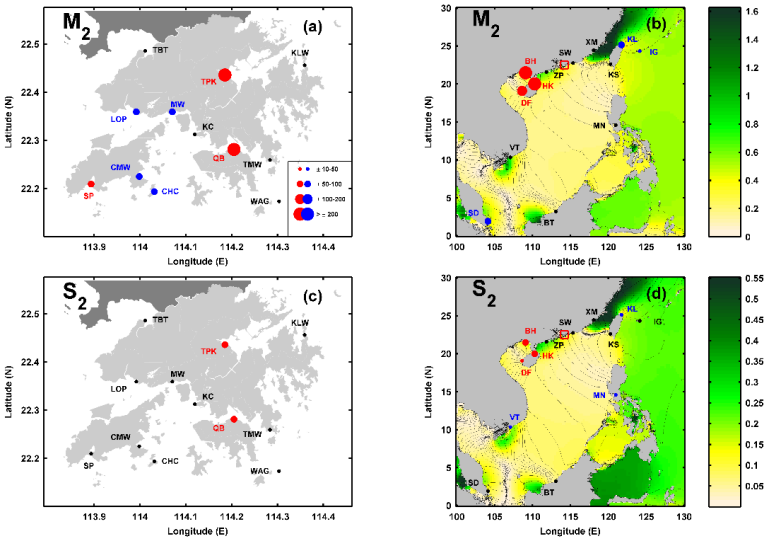

Figure 3 Semidiurnal tidal anomaly correlations (TACs) of detrended M_2 amplitude to detrended MSL in (a) Hong Kong, (b) the South China Sea, and of detrended S_2 amplitude to detrended MSL in (c) Hong Kong, and (d) the South China Sea. Red markers indicate positive TACs and blue indicates negative TACs, with the marker size showing the relative magnitude according to the legend. Black marks indicate insignificant TACs. Map backgrounds in (b) and (d) show mean tidal amplitudes over the period of 1993-2014 (color scale, meters) and phases (solid lines, 30° increment), taken from the ocean tidal model of TPXO7.2, (Egbert and Erofeeva, 2002, 2010).

Ocean Sci. Discuss., https://doi.org/10.5194/os-2018-62
Manuscript under review for journal Ocean Sci.
Discussion started: 11 June 2018

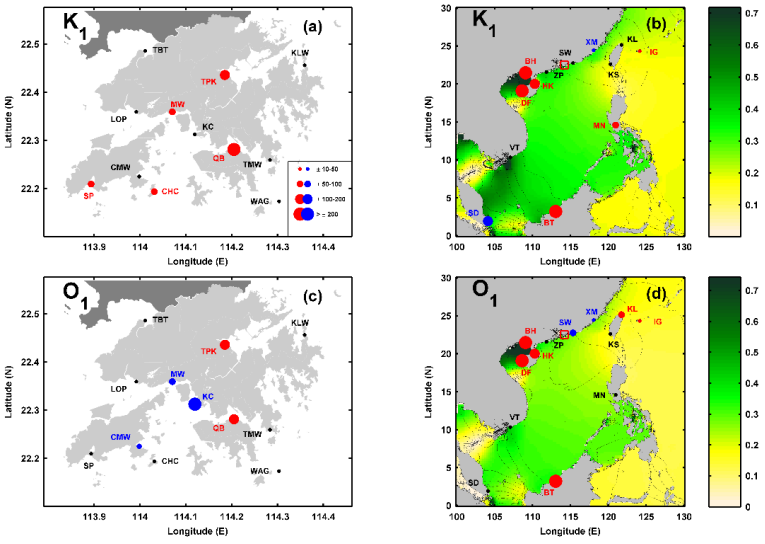

Figure 4 Diurnal tidal anomaly correlations (TACs) of detrended K_1 amplitude to detrended MSL in (a) Hong Kong, (b) the South China Sea, and of detrended O_1 amplitude to detrended MSL in (c) Hong Kong, and (d) the South China Sea. Red markers indicate positive TACs and blue indicates negative TACs, with the marker size showing the relative magnitude according to the legend. Black marks indicate insignificant TACs. Map backgrounds in (b) and (d) show mean tidal amplitudes over the period of 1993-2014 (color scale, meters) and phases (solid lines, 30° increment), taken from the ocean tidal model of TPXO7.2, (Egbert and Erofeeva, 2002, 2010).

Ocean Sci. Discuss., https://doi.org/10.5194/os-2018-62
Manuscript under review for journal Ocean Sci.
Discussion started: 11 June 2018

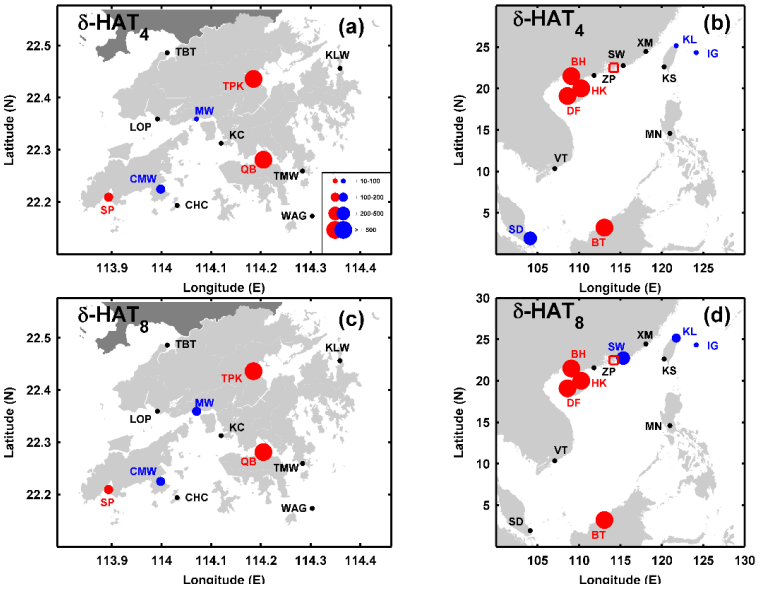

Figure 5 Results of the δ-HAT_4 determinations, the correlation of detrended (M_2 + S_2 + K_1 + O_1) to detrended MSL in Hong Kong (a) and the SCS (b), and results of the δ-HAT_8 determinations, the correlation of detrended (M_2 + S_2 + N_2 + K_2 + K_1 + O_1 + P_1 + Q_1) to detrended MSL in Hong Kong (c) and the SCS (d). Red markers indicate positive TACs and blue indicates negative TACs, with the marker size showing the relative magnitude according to the legend. Black marks indicate insignificant TACs.

Ocean Sci. Discuss., https://doi.org/10.5194/os-2018-62
Manuscript under review for journal Ocean Sci.
Discussion started: 11 June 2018

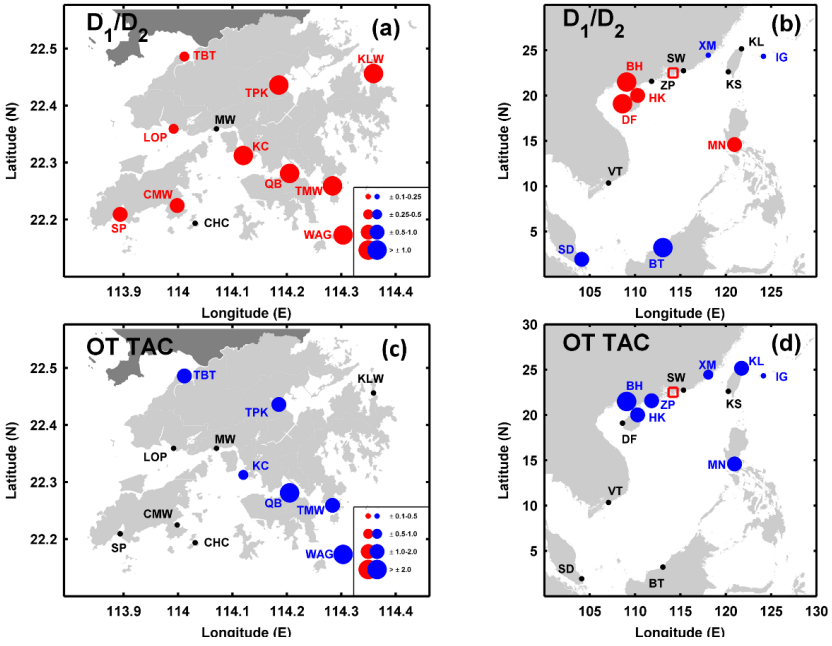

905

906 **Figure 6** Results of the D_1/D_2 TACs, the correlation of detrended D_2 ($M_2 + S_2 + N_2 + K_2$) to
907 detrended D_1 ($K_1 + O_1 + P_1 + Q_1$) in Hong Kong (a) and the SCS (b), and results of the OT
908 TACs, the correlation of detrended ($D_1 + D_2$) to detrended OT($M_4 + M_6 + MK_3 + MO_3 + MS_4$
909 + $MN_4 + S_4$) in Hong Kong (c) and the SCS (d). Red markers indicate positive TACs and
910 blue indicates negative TACs, with the marker size showing the relative magnitude according
911 to the legend. Black marks indicate insignificant TACs.

912

913

914

915

916

917

918

919

920

921

922

923

924

Ocean Sci. Discuss., https://doi.org/10.5194/os-2018-62
Manuscript under review for journal Ocean Sci.
Discussion started: 11 June 2018

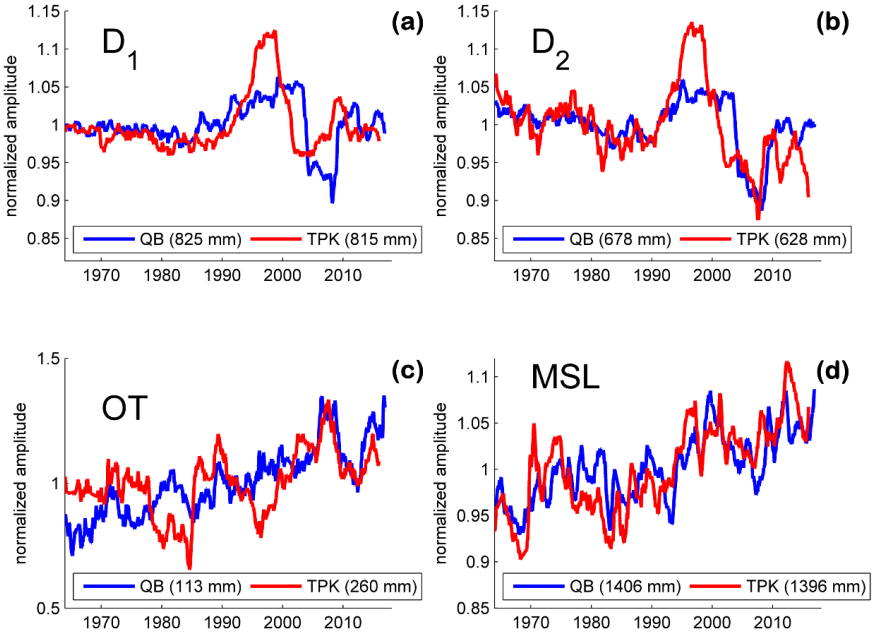

Figure 7 Time series of water level spectrum components at the Quarry Bay (QB; blue) and Tai Po Kau (TPK; red) tide gauges in Hong Kong, showing the D_1 band (a), the D_2 band (b), the OT band (c) and mean sea-level (MSL) (d). Components are plotted as a function of normalized amplitudes to show relative variability, with mean values given in the legend.

Ocean Sci. Discuss., https://doi.org/10.5194/os-2018-62
Manuscript under review for journal Ocean Sci.
Discussion started: 11 June 2018

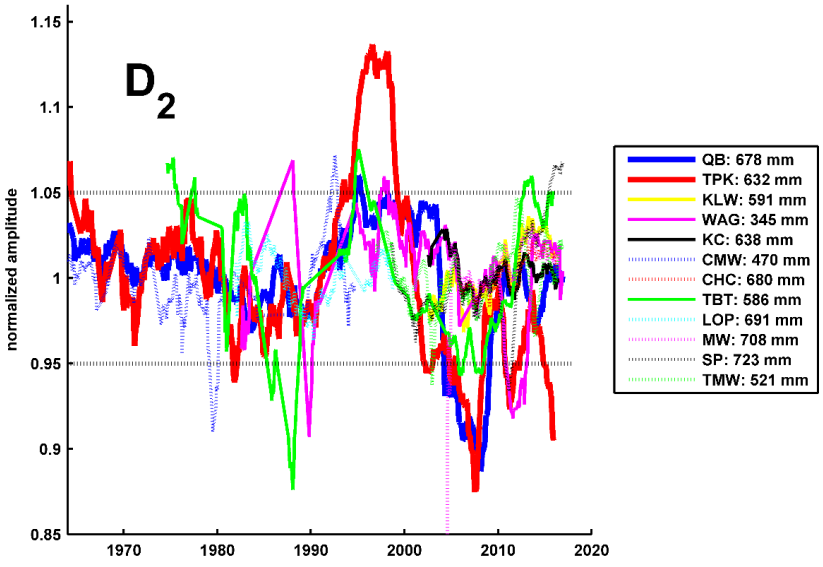

Figure 8 Time-series of detrended D_2 at all tide gauges in Hong Kong, plotted as a normalized amplitude to show relative variability, with mean values given in the legend. Each gauge is indicated by color according to the legend, with the QB (solid blue) and TPK (solid red) gauges shown as heavier lines. Horizontal dotted lines indicate the ±5% variational band relative to the mean amplitude.

Ocean Sci. Discuss., https://doi.org/10.5194/os-2018-62
Manuscript under review for journal Ocean Sci.
Discussion started: 11 June 2018

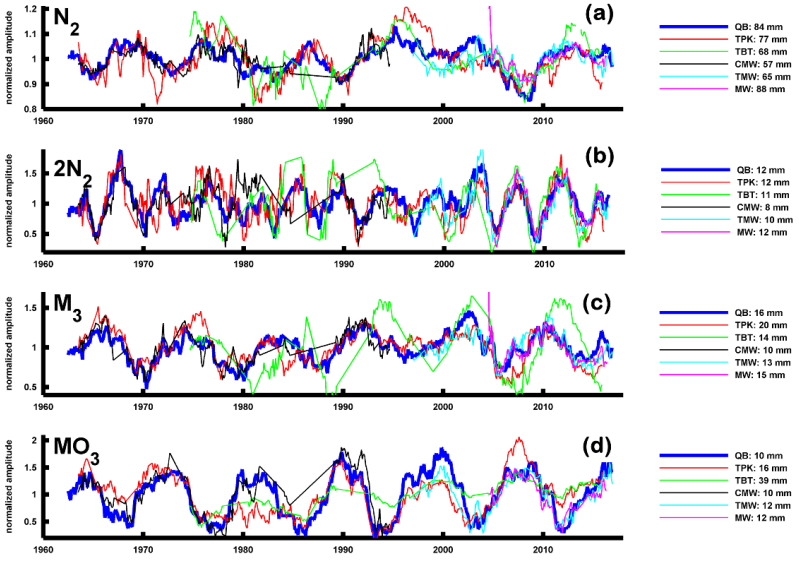

Figure 9 Minor constituent variability at selected Hong Kong gauges. N_2 is shown in (a), $2N_2$ in (b), M_3 in (c) and MO_3 in (d). All quantities are plotted as normalized amplitudes to show relative variability, with mean values given in the legends at the right.

Ocean Sci. Discuss., https://doi.org/10.5194/os-2018-62
Manuscript under review for journal Ocean Sci.
Discussion started: 11 June 2018

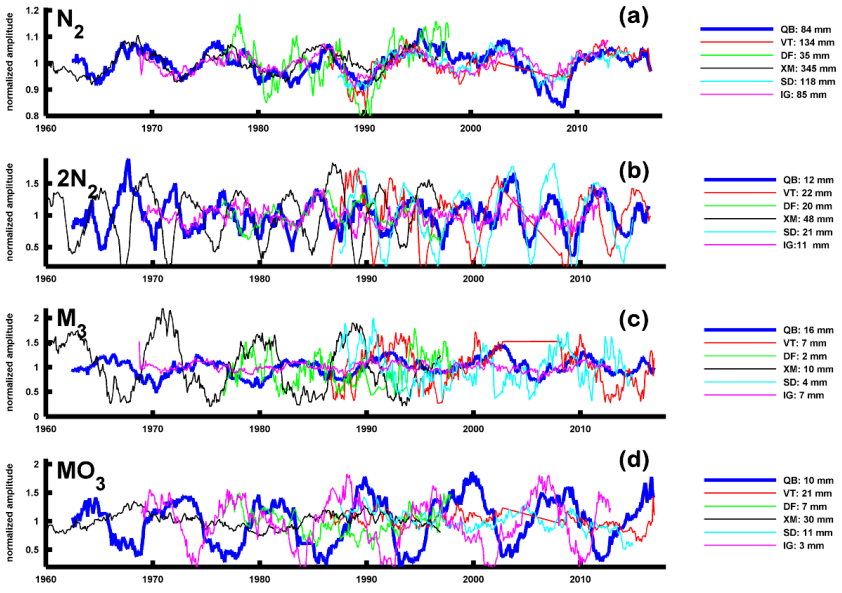

Figure 10 Minor constituent variability at selected South China Sea gauges. N_2 is shown in (a), $2N_2$ in (b), M_3 in (c) and MO_3 in (d). All quantities are plotted as normalized amplitudes to show relative variability, with mean values given in the legends at the right.

997 **REFERENCES:**

998 Alford, M. H. (2008). Observations of parametric subharmonic instability of the diurnal
999 internal tide in the South China Sea. *Geophysical Research Letters*, 35, L15602.
1000 doi:10.1029/2008GL034720

1001 Amin, M. (1983). On perturbations of harmonic constants in the Thames Estuary.
1002 Geophysical Journal of the Royal Astronomical Society. *73*(3): 587-603. doi:10.1111/j.1365-
1003 246X.1983.tb03334.x

1004 Arbic, B.K., Karsten, R.H., Garrett, C. (2009). On tidal resonance in the global ocean and the
1005 back-effect of coastal tides upon open-ocean tides. *Atmosphere-Ocean 47*(4), 239–266.
1006 doi:10.3137/OC311.2009

1007 Arns, A., Dangendorf, S., Jensen, J., Bender, J., Talke, S.A., & Pattiaratchi, C. (2017). Sea-
1008 level rise induced amplification of coastal protection design heights. *Nature: Scientific*
1009 *Reports,7*, 40171. doi:10.1038/srep40171

1010 Bowen, A. J., & Gray, D. A. (1972). The tidal regime of the River Thames; long-term trends
1011 and their possible causes. *Phil. Trans. R. Soc. Lond. A*, *272*(1221), 187-199.
1012 doi:10.1098/rsta.1972.0045

1013 Buchanan, M. K., Oppenheimer, M., & Kopp, R. E. (2017). Amplification of flood
1014 frequencies with local sea level rise and emerging flood regimes. *Environmental Research*
1015 *Letters*, *12*(6), 064009. doi:10.1088/1748-9326/aa6cb3.

1016 Carter, G.S. and M.C. Gregg (2006), Persistent near-diurnal internal waves observed above a
1017 site of M_2 barotropic-to-baroclinic conversion. *Journal of physical oceanography*, *36*(6),
1018 1136-1147. doi:10.1175/JPO2884.1

1019 Cartwright, D.E., & Tayler, R.J. (1971). New computations of the tide-generating potential.
1020 *Geophys. Journal of the Royal Astronomical Society*, *23*, 45-74. doi: 10.1111/j.1365-
1021 246X.1971.tb01803.x

1022 Cartwright, D.E. (1972). Secular changes in the oceanic tides at Brest, 1711–1936.
1023 *Geophysical Journal International*, 30(4), 433-449. doi:10.1.1.867.2468

1024 Cartwright, D.E., & Edden, A.C. (1973). Corrected tables of tidal harmonics. *Geophysical*
1025 *Research Letters, 33***,** 253-264. doi:10.1111/j.1365-246X.1973.tb03420.x

1026 Chernetsky, A. S., Schuttelaars, H. M., & Talke, S. A. (2010). The effect of tidal asymmetry
1027 and temporal settling lag on sediment trapping in tidal estuaries. *Ocean Dynamics*, *60*(5),
1028 1219-1241.. doi: 10.1007/s10236-010-0329-8

1029 Cherqui, F., Belmeziti, A., Granger, D., Sourdril, A., & Le Gauffre, P. (2015). Assessing
1030 urban potential flooding risk and identifying effective risk-reduction measures. *Science of the*
1031 *Total Environment*, *514*, 418-425.

1032 Chinn, B. S., Girton, J. B., & Alford, M. H. (2012). Observations of internal waves and
1033 parametric subharmonic instability in the Philippines archipelago. *Journal of Geophysical*
1034 *Research: Oceans*, *117*(C5). doi:10.1029/2011JC007392

1035 Church, J. A., & White, N. J. (2006). A 20th century acceleration in global sea-level
1036 rise. *Geophysical research letters*, *33*(1). doi:10.1029/2005GL024826

1037 Church, J. A., & White, N. J. (2011). Sea-level rise from the late 19th to the early 21st
1038 century. *Surveys in geophysics*, *32*(4-5), 585-602. doi 10.1007/s10712-011-9119-1

1039 Colosi, J. A., & Munk, W. (2006). Tales of the venerable Honolulu tide gauge. *Journal of*
1040 *physical oceanography*, *36*(6), 967-996. doi:10.1175/JPO2876.1

1041 Craik, A.D.D. (1985). Wave Interactions and Fluid Flows. Cambridge Univ. Press,
1042 Cambridge, U. K, ISBN: 978-0521368292

1043 Devlin, A. T., Jay, D. A., Talke, S. A., & Zaron, E. (2014). Can tidal perturbations associated
1044 with sea level variations in the western Pacific Ocean be used to understand future effects of
1045 tidal evolution? *Ocean Dynamics*, *64*(8), 1093-1120. doi:10.1007/s10236-014-0741-6

1046 Devlin, A.T., (2016). On the variability of Pacific Ocean Tides at seasonal to decadal time
1047 scale: Observed vs. modelled. *PhD thesis*, Portland State University

1048 Devlin, A. T., Jay, D. A., Zaron, E. D., Talke, S. A., Pan, J., & Lin, H. (2017). Tidal
1049 variability related to sea level variability in the Pacific Ocean. *Journal of Geophysical*
1050 *Research: Oceans*, *122*(11), 8445-8463. doi:10.1002/2017JC013165

1051 Devlin, A. T., Jay, D. A., Talke, S. A., Zaron, E. D., Pan, J., & Lin, H. (2017). Coupling of
1052 sea level and tidal range changes, with implications for future water levels. *Scientific*
1053 *Reports*, *7*(1), 17021. doi:10.1038/s41598-017-17056-z

1054 Devlin, A. T., Zaron, E. D., Jay, D. A., Talke, S. A., & Pan, J. (2018). Seasonality of Tides in
1055 Southeast Asian Waters. *Journal of Physical Oceanography*. doi: 10.1175/JPO-D-17-0119.1
1056 (accepted Feb. 2018)

1057 Domingues, C. M., Church, J. A., White, N. J., Gleckler, P. J., Wijffels, S. E., Barker, P. M.,
1058 & Dunn, J. R. (2008). Improved estimates of upper-ocean warming and multi-decadal sea-
1059 level rise. *Nature*, *453*(7198), 1090. doi:10.1038/nature07080

1060 Egbert, G. D., & Erofeeva, S. Y. (2002). Efficient inverse modeling of barotropic ocean
1061 tides. *Journal of Atmospheric and Oceanic Technology*, *19*(2), 183-204. doi: 10.1175/1520-
1062 0426(2002)019<0183: EIMOBO>2.0.CO; 2

1063 Egbert, G. D. & Erofeeva, S. Y. (2010). OTIS (OSU Tidal Inversion Software) TPXO7.2.
1064 College of Oceanic and Atmospheric Sciences, Oregon State University, Corvallis, Oregon,
1065 http://volkov.oce.orst.edu/tides/otis.html

1066 Haigh, I. D., Wijeratne, E. M. S., MacPherson, L. R., Pattiaratchi, C. B., Mason, M. S.,
1067 Crompton, R. P., & George, S. (2014). Estimating present day extreme water level
1068 exceedance probabilities around the coastline of Australia: tides, extra-tropical storm surges
1069 and mean sea level. *Climate Dynamics*, *42*(1-2), 121-138. doi: 10.1007/s00382-012-1652-1

1070 Familkhalili, R., & Talke, S. A. (2016). The effect of channel deepening on tides and storm
1071 surge: A case study of Wilmington, NC. *Geophysical Research Letters*, *43*(17), 9138-9147.
1072 doi:10.1002/2016GL069494

1073 Fang, G., Kwok, Y. K., Yu, K., & Zhu, Y. (1999). Numerical simulation of principal tidal
1074 constituents in the South China Sea, Gulf of Tonkin and Gulf of Thailand. *Continental Shelf*
1075 *Research*, *19*(7), 845-869. doi: 10.1016/S0278-4343(99)00002-3

1076 Feng, X., Tsimplis, M. N., & Woodworth, P. L. (2015). Nodal variations and long-term
1077 changes in the main tides on the coasts of China. *Journal of Geophysical Research:*
1078 *Oceans*, *120*(2), 1215-1232. doi:10.1002/2014JC010312

1079 Huthnance, J. M. (1980). On shelf-sea 'resonance' with application to Brazilian M3
1080 tides. *Deep Sea Research Part A. Oceanographic Research Papers*, *27*(5), 347-366.
1081 doi:10.1016/0198-0149(80)90031-X

1082 Ip, S.F. and H.G. Wai (1990), *An application of harmonic method to tidal analysis and*
1083 *prediction in Hong Kong*. Royal Observatory.

1084 Korobov, A. S., & Lamb, K. G. (2008). Interharmonics in internal gravity waves generated
1085 by tide-topography interaction. *Journal of Fluid Mechanics*, *611*, 61-95.
1086 doi:10.1017/S0022112008002449

1087 Jan, S., Chern, C. S., Wang, J., & Chao, S. Y. (2004). The anomalous amplification of M_2
1088 tide in the Taiwan Strait. *Geophysical Research Letters*, *31*(7). doi:10.1029/2003GL019373

1089 Jan, S., Chern, C. S., Wang, J., & Chao, S. Y. (2007). Generation of diurnal K_1 internal tide
1090 in the Luzon Strait and its influence on surface tide in the South China Sea. *Journal of*
1091 *Geophysical Research: Oceans*, *112*(C6). doi:10.1029/2006JC004003

1092 Jan, S., Lien, R. C., & Ting, C. H. (2008). Numerical study of baroclinic tides in Luzon
1093 Strait. *Journal of Oceanography*, *64*(5), 789. doi:10.1007/s10872-008-0066-5

1094 Jay, D. A. (2009). Evolution of tidal amplitudes in the eastern Pacific Ocean. *Geophysical*
1095 *Research Letters*, *36*(4). doi: 10.1029/2008GL036185

1096 Leffler, K. E., & Jay, D. A. (2009). Enhancing tidal harmonic analysis: Robust (hybrid
1097 L1/L2) solutions. *Continental Shelf Research*, *29*(1), 78-88. doi: 10.1016/j.csr.2008.04.011

1098 Li, K. W., & Mok, H. Y. (2012). Long term trends of the regional sea level changes in Hong
1099 Kong and the adjacent waters. In *Asian And Pacific Coasts 2011* (pp. 349-359).
1100 doi:10.1142/9789814366489_0040

1101 Lien, R. C., Tang, T. Y., Chang, M. H., & d'Asaro, E. A. (2005). Energy of nonlinear internal
1102 waves in the South China Sea. *Geophysical Research Letters*, *32*(5).
1103 doi:10.1029/2004GL022012

1104 Liu, Q., Xie, X., Shang, X., & Chen, G. (2016). Coherent and incoherent internal tides in the
1105 southern South China Sea. *Chinese journal of oceanology and limnology*, *34*(6), 1374-1382.
1106 doi:10.1007/s00343-016-5171-5

1107 MacKinnon, J. A., & Winters, K. B. (2005). Subtropical catastrophe: Significant loss of low-
1108 mode tidal energy at 28.9°. *Geophysical Research Letters*, *32*(15).
1109 doi:10.1029/2005GL023376

1110 Mawdsley, R. J., Haigh, I. D., & Wells, N. C. (2014). Global changes in mean tidal high
1111 water, low water and range. *Journal of Coastal Research*, *70*(sp1), 343-348.
1112 doi:10.2112/SI70-058.1

McComas, C. H., & Bretherton, F. P. (1977). Resonant interaction of oceanic internal waves. *Journal of Geophysical Research*, *82*(9), 1397-1412. doi:10.1029/JC082i009p01397

Mercier, M. J., Mathur, M., Gostiaux, L., Gerkema, T., Magalhães, J. M., Da Silva, J. C., & Dauxois, T. (2012). Soliton generation by internal tidal beams impinging on a pycnocline: laboratory experiments. *Journal of Fluid Mechanics*, *704*, 37-60. doi:10.1017/jfm.2012.191

Moftakhari, H. R., AghaKouchak, A., Sanders, B. F., Feldman, D. L., Sweet, W., Matthew, R. A., & Luke, A. (2015). Increased nuisance flooding along the coasts of the United States due to sea level rise: Past and future. *Geophysical Research Letters*, *42*(22), 9846-9852. doi:10.1002/2015GL066072

Moftakhari, H. R., AghaKouchak, A., Sanders, B. F., & Matthew, R. A. (2017). Cumulative hazard: The case of nuisance flooding. *Earth's Future*, *5*(2), 214-223. doi:10.1002/2016EF000494

Müller, M., Arbic, B. K., & Mitrovica, J. X. (2011). Secular trends in ocean tides: Observations and model results. *Journal of Geophysical Research: Oceans*, *116*(C5). doi:10.1029/2010JC006387

Müller, M., Cherniawsky, J. Y., Foreman, M. G. G., & Storch, J. S. (2012). Global M_2 internal tide and its seasonal variability from high resolution ocean circulation and tide modeling. *Geophysical Research Letters*, *39*(19). doi:10.1029/2012GL053320

Müller, M. (2012). The influence of changing stratification conditions on barotropic tidal transport and its implications for seasonal and secular changes of tides. *Continental Shelf Research*, *47*, 107-118. doi: 10.1016/j.csr.2012.07.003

Niwa, Y., & Hibiya, T. (2004). Three-dimensional numerical simulation of M_2 internal tides in the East China Sea. *Journal of Geophysical Research: Oceans*, *109*(C4). doi:10.1029/2003JC001923

Pawlowicz, R., Beardsley, B., & Lentz, S. (2002). Classical tidal harmonic analysis including error estimates in MATLAB using T_TIDE. *Computers & Geosciences*, *28*(8), 929-937. doi:10.1016/S0098-3004(02)00013-4

Rasheed, A. S., & Chua, V. P. (2014). Secular trends in tidal parameters along the coast of Japan. *Atmosphere-Ocean*, *52*(2), 155-168. doi:10.1080/07055900.2014.886031

Ray, R. D. (2006). Secular changes of the M_2 tide in the Gulf of Maine. *Continental shelf research*, *26*(3), 422-427. doi: 10.1016/j.csr.2005.12.005

Ray, R. D., & Foster, G. (2016). Future nuisance flooding at Boston caused by astronomical tides alone. *Earth's Future*, *4*(12), 578-587. doi:10.1002/2016EF000423

Ross, A. C., Najjar, R. G., Li, M., Lee, S. B., Zhang, F., & Liu, W. (2017). Fingerprints of Sea Level Rise on Changing Tides in the Chesapeake and Delaware Bays. *Journal of Geophysical Research: Oceans*, *122*(10), 8102-8125. doi:10.1002/2017JC012887

Teoh, S. G., Ivey, G. N., & Imberger, J. (1997). Laboratory study of the interaction between two internal wave rays. *Journal of Fluid Mechanics*, *336*, 91-122. doi:10.1017/S0022112096004508

Vellinga, N. E., Hoitink, A. J. F., van der Vegt, M., Zhang, W., & Hoekstra, P. (2014). Human impacts on tides overwhelm the effect of sea level rise on extreme water levels in the Rhine–Meuse delta. *Coastal Engineering*, *90*, 40-50. doi: 10.1016/j.coastaleng.2014.04.005

Webb, D. J. (1976, January). A model of continental-shelf resonances. In *Deep Sea Research and Oceanographic Abstracts* (Vol. 23, No. 1, pp. 1-15). Elsevier. doi:10.1016/0011-7471(76)90804-4

Woodworth, P. L. (2010). A survey of recent changes in the main components of the ocean tide. *Continental Shelf Research*, *30*(15), 1680-1691. doi: 10.1016/j.csr.2010.07.002

Xie, X. H., Chen, G. Y., Shang, X. D., & Fang, W. D. (2008). Evolution of the semidiurnal (M2) internal tide on the continental slope of the northern South China Sea. *Geophysical Research Letters*, *35*(13). doi:10.1029/2008GL034179

Xie, X. H., Shang, X. D., van Haren, H., Chen, G. Y., & Zhang, Y. Z. (2011). Observations of parametric subharmonic instability-induced near-inertial waves equatorward of the critical diurnal latitude. *Geophysical Research Letters*, *38*(5). doi:10.1029/2010GL046521

Xie, X., Shang, X., Haren, H., & Chen, G. (2013). Observations of enhanced nonlinear instability in the surface reflection of internal tides. *Geophysical Research Letters*, *40*(8), 1580-1586. doi:10.1002/grl.50322

Xing, J., & Davies, A. M. (2002). Processes influencing the non-linear interaction between inertial oscillations, near inertial internal waves and internal tides. *Geophysical Research Letters*, *29*(5). doi:10.1029/2001GL014199

Zaron, E. D., & Jay, D. A. (2014). An analysis of secular change in tides at open-ocean sites in the Pacific. *Journal of Physical Oceanography*, *44*(7), 1704-1726. doi:10.1175/JPO-D-13-0266.1

1175 Zhang, H., Wang, T., Liu, M., Jia, M., Lin, H., Chu, L. M., & Devlin, A. T. (2018). Potential
1176 of Combining Optical and Dual Polarimetric SAR Data for Improving Mangrove Species
1177 Discrimination Using Rotation Forest. *Remote Sensing*, *10*(3), 467. doi: 10.3390/rs10030467

1178 Zu, T., Gan, J., & Erofeeva, S. Y. (2008). Numerical study of the tide and tidal dynamics in
1179 the South China Sea. *Deep Sea Research Part I: Oceanographic Research Papers*, *55*(2),
1180 137-154. doi: 10.1016/j.dsr.2007.10.007

1181
1182
1183
1184
1185
1186
1187
1188
1189
1190
1191
1192
1193
1194
1195
1196
1197
1198
1199
1200
1201
1202
1203
1204

Ocean Sci. Discuss., https://doi.org/10.5194/os-2018-62
Manuscript under review for journal Ocean Sci.
Discussion started: 11 June 2018

TABLES:

Table 1 Metadata for all tide gauge locations, giving latitude/longitude, and star year/end year of data analyzed. Except where indicated by country code, all locations are located in the People's Republic of China (PRC). The solid horizontal line demarcates Hong Kong and South China Sea tide gauges.

Station	*Latitude*	*Longitude*	*Start Year*	*End Year*
Quarry Bay (QB)	22.27° N	114.21° E	1954	2016
Tai Po Kau (TPK)	22.42° N	114.19° E	1963	2016
Tsim Bei Tusi (TBT)	22.48° N	114.02° E	1974	2016
Chi Ma Wan (CMW)	22.22° N	114.00° E	1963	1997
Cheung Chau (CHC)	22.19° N	114.03° E	2004	2016
Lok On Pai (LOP)	22.35° N	114.00° E	1981	1999
Ma Wan (MW)	22.35° N	114.06° E	2004	2016
Tai Miu Wan (TMW)	22.26° N	114.29° E	1996	2016
Shek Pik (SP)	22.21° N	113.89° E	1999	2016
Waglan Island (WAG)	22.17° N	114.30° E	1995	2016
Ko Lau Wan (KLW)	22.45° N	114.34° E	2004	2016
Kwai Chung (KC)	22.31° N	114.12° E	2004	2016
Dongfang (DF)	19.10° N	108.62° E	1975	1997
Beihei (BH)	21.48° N	109.08° E	1975	1997
Haikou (HK)	20.02° N	110.28° E	1976	1997
Zhapo (ZP)	21.58° N	111.83° E	1975	1997
Shanwei (SW)	22.75° N	115.35° E	1975	1997
Xiamen (XM)	24.45° N	118.07° E	1954	1997
Keelung (KL)	22.62° N	120.29° E	1980	2014
Kaohsiung (KS)	25.16° N	121.75° E	1980	2014
Manila, PHL (MN)	14.59° N	120.97° E	1984	2016
Vung Tau, VTM (VT)	10.34° N	107.07° E	1986	2014*
Sedili, MLY (SD)	1.93° N	104.12° E	1986	2016
Bintulu, MLY (BT)	3.22° N	113.07° E	1992	2016
Ishigaki, JPN (IG)	24.33° N	124.15° E	1968	2013

*-missing data from 2002-2007

Ocean Sci. Discuss., https://doi.org/10.5194/os-2018-62
Manuscript under review for journal Ocean Sci.
Discussion started: 11 June 2018

Table 2 Amplitude TACs for M_2, S_2, K_1, and O_1. All values given are in units of milimeter change in tidal amplitude for a 1-meter fluctuation in sea-level (mm m^{-1}). Statistically significant positive values are given in bold italic text.

Station	**M_2 TAC**	**S_2 TAC**	**K_1 TAC**	**O_1 TAC**
Quarry Bay (QB)	***+218 ± 37***	***+85 ± 16***	***+220 ± 15***	***+146 ± 11***
Tai Po Kau (TPK)	***+267 ± 42***	***+98 ± 17***	***+190 ± 68***	***+100 ± 25***
Tsim Bei Tusi (TBT)	+7 ± 80	-10 ± 15	+32 ± 22	+24 ± 22
Chi Ma Wan (CMW)	***-58 ± 11***	-7 ± 5	-18 ± 8	***-37 ± 10***
Cheung Chau (CHC)	***-63 ± 20***	-22 ± 35	***+69 ± 48***	+50 ± 92
Lok On Pai (LOP)	***-81 ± 24***	-18 ± 8	+8 ± 32	-24 ± 12
Ma Wan (MW)	***-68 ± 4***	+1 ± 25	***+52 ± 4***	***-62 ± 21***
Tai Miu Wan (TMW)	+22 ± 59	-1 ± 9	+10 ± 22	+3 ± 8
Shek Pik (SP)	***+62 ± 29***	+11 ± 18	***+70 ± 4***	+28 ± 17
Waglan Island (WAG)	+1 ± 21	+3 ± 6	+9 ± 7	-9 ± 8
Ko Lau Wan (KLW)	-46 ± 39	-11 ± 17	+29 ± 65	+60 ± 57
Kwai Chung (KC)	-90 ± 46	-10 ± 29	-91 ± 226	***-202 ± 161***
Dongfang (DF)	***+190 ± 75***	***+43 ± 9***	***+482 ± 53***	***+320 ± 52***
Beihei (BH)	***+461 ± 170***	***+88 ± 19***	***+579 ± 152***	***+294 ± 78***
Haikou (HK)	***+379 ± 106***	***+55 ± 8***	***+180 ± 28***	***+194 ± 37***
Zhapo (ZP)	-32 ± 30	-12 ± 30	+40 ± 33	+1 ± 44
Shanwei (SW)	+30 ± 30	-34 ± 31	-26 ± 15	***-79 ± 53***
Xiamen (XM)	+93 ± 31	-32 ± 35	***-46 ± 4***	***-48 ± 8***
Keelung (KL)	***-69 ± 14***	***-37 ± 5***	-4 ± 8	***+21 ± 4***
Kaohsiung (KS)	+25 ± 8	+1 ± 18	+1 ± 8	+28 ± 16
Manila, PHL (MN)	-17 ± 16	***-21 ± 9***	***+83 ± 12***	-20 ± 16
Vung Tau, VTM (VT)	+21 ± 26	***-44 ± 7***	+7 ± 21	+20 ± 6
Sedili, MLY (SD)	***-72 ± 35***	+24 ± 24	***-148 ± 35***	-54 ± 33
Bintulu, MLY (BT)	-37 ± 15	+11 ± 7	***+291 ± 45***	***+320 ± 36***
Ishigaki, JPN (IG)	***-46 ± 2***	-8 ± 7	***+23 ± 11***	+1 ± 11

Ocean Sci. Discuss., https://doi.org/10.5194/os-2018-62
Manuscript under review for journal Ocean Sci.
Discussion started: 11 June 2018

Table 3 The δ-HAT$_4$, δ-HAT$_8$, D_1/D_2 TACs, and OT TACs. The δ-HAT values given are in units of milimeter change in tidal amplitude for a 1-meter fluctuation in sea-level (mm m^{-1}). D_1/D_2 and OT TACs are in unitless ratios (i.e., mm mm^{-1}) Statistically significant positive values are given in bold italic text.

Station	**δ-HAT$_4$**	**δ-HAT$_8$**	**D_1/D_2**	**OT/ (D_1 + D_2)**
Quarry Bay (QB)	***+665 ± 82***	***+834 ± 108***	***+1.08 ± 0.05***	***-3.62 ± 0.99***
Tai Po Kau (TPK)	***+612 ± 210***	***+797 ± 138***	***+1.01 ± 0.04***	***-1.87 ± 0.10***
Tsim Bei Tusi (TBT)	+56 ± 117	+41 ± 180	***+0.37 ± 0.02***	***-1.69 ± 0.14***
Chi Ma Wan (CMW)	***-119 ± 19***	***-159 ± 28***	***+0.74 ± 0.19***	-0.01 ± 0.60
Cheung Chau (CHC)	-12 ± 42	+224 ± 646	+0.81 ± 1.03	-0.11 ± 1.36
Lok On Pai (LOP)	-114 ± 45	-112 ± 110	***+0.26 ± 0.05***	-0.26 ± 0.21
Ma Wan (MW)	***-91 ± 73***	***-117 ± 35***	+0.57 ± 1.02	-0.42 ± 1.44
Tai Miu Wan (TMW)	+42 ± 100	+89 ± 99	***+1.04 ± 0.20***	***-1.31 ± 0.23***
Shek Pik (SP)	***+138 ± 37***	***+183 ± 20***	***+0.89 ± 0.06***	-0.01 ± 0.60
Waglan Island (WAG)	+3 ± 31	+4 ± 30	***+1.11 ± 0.17***	***-3.05 ± 0.43***
Ko Lau Wan (KLW)	-66 ± 47	+83 ± 367	***+1.31 ± 0.62***	-0.35 ± 0.82
Kwai Chung (KC)	-55 ± 64	+270 ± 730	***+1.19 ± 0.60***	***-0.62 ± 0.42***
Dongfang (DF)	***+1037 ± 453***	***+1236 ± 113***	***+2.86 ± 0.19***	***-6.10 ± 2.69***
Beihei (BH)	***+1405 ± 453***	***+2190 ± 151***	***+1.22 ± 0.03***	***-5.21 ± 0.15***
Haikou (HK)	***+813 ± 217***	***+1086 ± 189***	***+0.61 ± 0.05***	***-1.75 ± 0.04***
Zhapo (ZP)	-34 ± 111	-16 ± 69	+0.14 ± 0.07	***-1.69 ± 0.57***
Shanwei (SW)	-94 ± 94	***-217 ± 150***	+0.02 ± 0.18	-0.09 ± 0.20
Xiamen (XM)	+54 ± 38	-3 ± 43	***+0.12 ± 0.04***	***-0.92 ± 0.23***
Keelung (KL)	***-95 ± 21***	***-125 ± 44***	+0.08 ± 0.11	***-1.29 ± 0.57***
Kaohsiung (KS)	+54 ± 36	+52 ± 83	+0.16 ± 0.07	-1.55 ± 0.74
Manila, PHL (MN)	+39 ± 67	+5 ± 53	***+0.81 ± 0.61***	***-1.86 ± 0.49***
Vung Tau, VTM (VT)	-28 ± 22	-11 ± 59	+0.15 ± 0.08	+0.40 ± 0.59
Sedili, MLY (SD)	***-254 ± 70***	-76 ± 55	***-0.63 ± 0.06***	***-1.33 ± 0.50***
Bintulu, MLY (BT)	***+600 ± 52***	**+942 ± 55**	***-3.81 ± 1.60***	+1.62 ± 0.98
Ishigaki, JPN (IG)	***-58 ± 6***	+4 ± 24	***-0.12 ± 0.09***	+0.31 ± 0.61

Ocean Sci. Discuss., https://doi.org/10.5194/os-2018-62
Manuscript under review for journal Ocean Sci.
Discussion started: 11 June 2018

1257 **Table 4** Correlations of tidal components with the North Point/Quarry Bay (QB) tide gauge,
1258 showing M_2, K_1, N_2, $2N_2$, M_3, and MO_3. Two numbers are given in each column,
1259 representing the correlations in the "historical" era (pre-1997), and the "modern" era (post-
1260 1997). Non-existent data is indicated by "~". An average value is also calculated at the local
1261 (Hong Kong) and regional (South China Sea) scale for each era. Data records that cover both
1262 time periods will indicate the better correlated era by bold text. Other tidal component
1263 correlations (including MSL) are given in Table S3 in the supplementary material.

Station	**M_2**	**K_1**	**N_2**	**$2N_2$**	**M_3**	**MO_3**
TPK	**0.83**/0.56	**0.72**/0.30	**0.71**/0.57	0.54/**0.73**	0.76/**0.77**	0.74/**0.78**
TBT	0.58/**0.77**	**0.48**/0.19	0.72/**0.78**	0.48/**0.70**	0.45/**0.52**	0.66/**0.78**
CMW/CHC	0.49/**0.56**	**0.42**/0.21	**0.69**/0.61	0.61/**0.94**	**0.88**/0.80	**0.92**/0.90
LOP/MW	**0.57**/0.11	**0.55**/0.16	**0.87**/0.76	0.74/**0.95**	**0.85**/0.29	**0.88**/0.87
TMW	~/0.25	~/0.60	~/0.65	~/0.87	~/0.76	~/0.93
SP	~/0.30	~/0.56	~/0.59	~/0.83	~/0.59	~/0.83
WAG	~/0.22	~/0.52	~/0.62	~/0.82	~/0.76	~/0.90
KC	~/0.20	~/0.25	~/0.76	~/0.93	~/0.82	~/0.92
KLW	~/0.16	~/-0.02	~/0.70	~/0.92	~/0.76	~/0.94
HK Ave.	**0.62**/0.28	**0.54**/0.31	**0.75**/0.67	0.59/**0.86**	**0.74**/0.67	0.80/**0.88**
DF	0.78/~	0.62/~	0.63/~	0.63/~	-0.32/~	-0.27/~
BH	0.75/~	0.58/~	0.55/~	0.35/~	-0.03/~	0.13/~
HK	0.82/~	0.53/~	0.61/~	0.27/~	0.18/~	0.21/~
ZP	0.34/~	0.68/~	0.78/~	0.12/~	0.75/~	0.64/~
SW	0.73/~	0.32/~	0.83/~	0.77/~	0.84/~	0.89/~
XM	-0.49/~	0.24/~	0.61/~	-0.47/~	-0.63/~	-0.15/~
KL	~/-0.32	~/-0.13	~/0.49	~/0.18	~/0.45	~/-0.37
KS	~/0.34	~/0.62	~/0.53	~/0.53	~/0.14	~/-0.10
MN	~/-0.16	~/-0.07	~/0.06	~/0.50	~/0.48	~/0.35
VT	~/0.49	~/0.63	~/0.56	~/0.08	~/0.54	~/-0.03
SD	~/0.40	~/-0.46	~/0.80	~/0.79	~/-0.03	~/-0.31
BT	~/0.10	~/0.54	~/0.19	~/0.21	~/0.19	~/-0.17
IG	0.18/**0.36**	**0.38**/0.07	0.62/**0.72**	0.34/**0.54**	**0.52**/0.47	-0.17/**0.08**
SCS Ave.	**0.45**/0.17	**0.48**/0.17	**0.66**/0.48	0.29/**0.41**	0.19/**0.32**	**0.12**/-0.09

1264

1265

1266